# Supporting Information

# Experimental and Theoretical Studies of a Spirostannole and Formation of a Pentaorganostannate †

**Isabel-Maria Ramirez y Medina [1,2], Markus Rohdenburg [1,3], Waldemar Kipke [1,4], Enno Lork [1,5] and Anne Staubitz [1,6,*]**

[1] MAPEX Center for Materials and Processes, University of Bremen, Bibliothek Str. 1, 28359 Bremen, Germany

[2] Institute for Organic and Analytical Chemistry, University of Bremen, Leobener Str. 7, 28359 Bremen, Germany; ramirez-y-medina@uni-bremen.de

[3] Institute for Applied and Physical Chemistry, University of Bremen, Leobener Str. 5, 28359 Bremen, Germany; m.rohdenburg@uni-bremen.de

[4] Institute for Organic and Analytical Chemistry, University of Bremen, Leobener Str. 7, 28359 Bremen, Germany; kipke@uni-bremen.de

[5] Institute for Inorganic Chemistry and Crystallography, University of Bremen, Leobener Str. 7, 28359 Bremen, Germany; elo@uni-bremen.de

[6] Institute for Organic and Analytical Chemistry, University of Bremen, Leobener Str. 7, 28359 Bremen, Germany

* Correspondence: staubitz@uni-bremen.de

† In memory of Hans J. Reich

# Table of Contents

# 1. General Considerations

## 1.1 Abbreviations

| | |
|---|---|
| calcd. | calculated |
| Cu(I)Cl | copper(I) chloride |
| Cu(I)I | copper(I) iodide |
| DCM | dichloromethane |
| DFT | density functional theory |
| EI | electron impact |
| $Et_2O$ | diethyl ether |
| EtOAc | ethyl acetate |
| EtOH | ethanol |
| GB | glove box |
| HOMO | highest occupied molecular orbital |
| IR | infrared spectroscopy |
| LUMO | lowest unoccupied molecular orbital |
| MCP-PMT detector | micro-channel plate (MCP)-photomultiplier tubes (PMT) detector |
| MeOH | methanol |
| NIS | *N*-iodosuccinimide |
| NMR | nuclear magnetic resonance |
| $[PdCl_2(PPh_3)_2]$ | bis(triphenylphosphine)palladium(II) dichloride |
| PFK | perfluorokerosene |
| ppm | parts per million |
| R | resolution (for mass spectrometry) |

| | |
|---|---|
| sat. soln. | saturated solution |
| SPS | solvent purification system |
| TCSPC | time-correlated single photon counting |
| TEA | triethylamine |
| THF | tetrahydrofuran |
| TLC | thin layer chromatography |
| TMS | tetramethylsilane |

## 1.2 Chemicals and Solvents

Reactions under inert conditions were carried out using standard Schlenk techniques under a dry, inert $N_2$ or Ar atmosphere or in a $N_2$-filled glove box from Inert. All anhydrous solvents were taken from the solvent purification system (SPS), degassed by four freeze-pump-thaw cycles and stored under a $N_2$ atmosphere. All chemicals were commercially available and were used without further purification unless noted otherwise.

**Table S1.** List of supplier and purity of used chemicals.

| Reagent | Supplier | Purity | Comments |
|---|---|---|---|
| Ammonium chloride | Carl Roth | ≥ 99.5% | |
| Copper(I) chloride | Alfa Aesar | 99.999% | stored in a GB |
| Copper(I) iodide | Alfa Aesar | 99.998% | stored in a GB |
| *N*-Iodosuccinimide | Sigma-Aldrich | 98% | |
| Magnesium sulfate | Grüssing | 99% | |
| Methyllithium | Acros Organics | | 1.6 M in diethyl ether |
| 2-Methylthiophene | Sigma-Aldrich | 98% | |
| 1,7-Octadiyne | VWR Chemicals | 98% | |
| $[PdCl_2(PPh_3)_2]$ | Strem Chemicals | 99.9+% | |
| Sodium carbonate | Sigma-Aldrich | 99.5% | |
| Sodium thiosulfate | Grüssing | 97% | |
| Tin(IV) chloride | Sigma Aldrich | | 1 M in heptanes under $N_2$ atmosphere |
| *p*-Toluenesulfonic acid·$H_2O$ | Acros Organics | 97.5 % | |

**Table S2.** List of suppliers and purity of used solvents.

| Solvent | Comments |
|---|---|
| Dichloromethane | VWR Chemicals; for HPLC; anhydrous from the SPS |
| Diethyl ether | VWR Chemicals; ACS, Reag. Ph. Eur. |
| Ethyl acetate | VWR Chemicals; ACS, Reag. Ph. Eur. |
| Ethanol | VWR Chemicals; Ethanol absolute ≥99.8% |
| *n*-Pentane | VWR Chemicals; ACS, Reag. Ph. Eur. |
| Triethylamine | Sigma Aldrich; 99%; anhydrous; degassed |
| Tetrahydrofuran | VWR Chemicals; for HPLC; anhydrous from the SPS and degassed |
| Toluene | VWR Chemicals; for HPLC; anhydrous, from the SPS and degassed |

## 1.3 Analytical Instruments

$^1H$, $^{13}C\{^1H\}$, $^7Li$ and $^{119}Sn\{^1H\}$ NMR spectra were recorded on a *Bruke*r Avance Neo 600 or *Bruke*r DRX 500 at 25°C unless noted otherwise. All $^1H$ NMR and $^{13}C\{^1H\}$ NMR spectra were referenced against the solvent residual proton signals ($^1H$), or the solvent itself ($^{13}C$). The reference for the $^7Li$ and $^{119}Sn\{^1H\}$ NMR spectra was calculated based on the $^1H$ NMR spectrum of TMS. All chemical $\delta$ shifts are given in parts per million (ppm) and all coupling constants $J$ in Hz. The following abbreviations are used to describe splitting patterns: br s = broad singlet, s = singlet, d = doublet, dd = doublet of doublets, m = multiplet.

Electron Impact (EI) ionisation mass spectra were obtained on the double focusing mass spectrometer MAT 95XL. Samples were measured by direct inlet or indirect inlet method with a source temperature of 200° C. The ionisation energy of the electron impact ionisation was 70 eV. All signals were reported with the quotient from mass to charge $m/z$. High resolution (HR) EI mass

spectra were recorded on the double focusing mass spectrometer MAT 95XL from FINNIGAN MAT. Precision weights were determined via the peak-matching method. The reference substance was perfluorokerosene (PFK). The resolution (R) of the peak-matching performance was 10000. The calculated isotopic distribution for each ion agreed with experimental values.

IR spectra were recorded on a *Nicolet* Thermo IS10 SCIENTIFIC spectrometer with a diamond ATR unit. The resolution was 4 $cm^{-1}$. Relative intensities of the IR bands were described by s = strong (0 – 33% T), m = medium (34 – 66% T) or w = weak (67 – 100% T).

All melting points were measured with a *Büchi* Melting Point M-560 apparatus and are uncorrected.

Thin layer chromatography (TLC) was carried out on aluminum plates from Macherey-Nagel that were coated with silica gel 60 $F_{254}$ with a layer thickness of 0.2 mm. All bands were detected by using UV light (254 nm and 366 nm). Column chromatography was carried out by using the column machine PuriFlash 4250 from Interchim. Silica gel columns of the type PF-15SiHP-F0025 and PF-50SiHP-JP-F0120 were used. The injection of the sample was performed via dry load. The column material of the dry load was Celite 503 from Macherey-Nagel.

UV/Vis spectra were recorded with a resolution of 0.1 nm on a UV-2700 spectrometer from *Shimadzu*.

Emission spectra were recorded on an Edinburgh Instruments FLS 1000 photoluminescence spectrometer. Absolute quantum yields (QY) were measured with an Edinburgh Instruments integrating sphere. TCSPC measurements were performed using a fast response MCP-PMT detector and a 376 nm Edinburgh Instruments EPL Laser as excitation source with 10 – 20 MHz repetition rate and 80 ps pulse width. Temperature dependent-fluorescence measurements were carried out using an Oxford Instruments Optistat-CF cryostat cooled with liquid nitrogen. All emission spectra are corrected spectra.

Cyclic voltammetry measurements were carried out using the potentiostat Autolab PGSTAT101 Metrohm. The material of the working electrode and the counter electrode was platinum. The material of the reference electrode was silver; all spectra were referenced against ferrocene. The scan rate was 0.2 V/s. The solvent was dichloromethane and the conducting salt was tetrabutylammonium hexafluorophosphate (TBA[$PF_6$] 0.1 M).

## 1.4 Crystallography

Intensity data of **4** was collected on a Bruker Venture D8 diffractometer at 100 K with Mo-Kα (0.7107 Å) radiation. All structures were solved by direct methods and refined based on $F^2$ by use of the SHELX[1-2] program package as implemented in OLex2 1.2.[3] All non-hydrogen atoms were refined using anisotropic displacement parameters. Hydrogen atoms attached to carbon atoms were included in geometrically calculated positions using a riding model. Crystal and refinement data are collected in Table S3. Figures were created using DIAMOND.

Crystallographic data for the structural analyses have been deposited within Cambridge Crystallographic Data Centre. Copies of this information may be obtained free of charge from the Director, CCDC, 12 Union Road, Cambridge CB2 1EZ, UK (Fax: +44-1223-336033; e-mail: deposit@ccdc.cam.ac.uk or http://www.ccdc.cam.ac.uk).

# 2. Syntheses

## 2.1 2-Iodo-5-methylthiophene (1)[4]

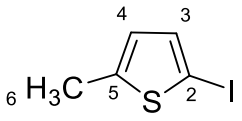


This reaction was carried out under normal atmosphere. To a solution of 2-methylthiophene (5.00 g, 50.9 mmol) in EtOH (70 mL), NIS (12.6 g, 56.0 mmol) and *p*-toluenesulfonic acid (970 mg, 5.09 mmol, 10 mol%) were added at 22 °C. The reaction mixture was stirred at 22 °C for 10 min and a sat. soln. of $Na_2S_2O_3$ (88 mL) was added. It was extracted with EtOAc (3 x 100 mL) and the organic phase was separated. It was washed with a 1 M solution of $Na_2CO_3$ (100 mL), dried over $MgSO_4$, filtered, and dried *in vacuo*. Purification by Kugelrohr distillation (85 °C, 11 mbar) gave the product as a light yellow oil (11.4 g, 61%). $^1$H NMR (500 MHz, $CDCl_3$): δ 7.03 (d, $^3J_{HH}$ = 3.5 Hz, 1H, H-3), 6.46 (d, $^3J_{HH}$ = 3.5 Hz, 1H, H-4), 2.48 (s, 3H, H-6) ppm; $^{13}$C{$^1$H} NMR (126 MHz, $CDCl_3$): δ 146.1 (C-5), 136.9 (C-3), 127.1 (C-4), 69.5 (C-2), 15.5 (C-6) ppm; IR (ATR): *ν* 2917 (w), 2855 (w), 1538 (w), 1432 (m), 1213 (m), 1158 (m), 1050 (w), 982 (w), 929 (m), 786 (s), 737 (w), 695 (w), 664 (m) cm$^{-1}$; HR-MS (EI, $C_5H_5IS$) calcd. 223.91512, found 223.91511 (R = 10000); MS (EI, 70 eV, indirect inlet, 200 °C): *m*/*z* (% relative intensity) = 224 (100) $[M]^{+\cdot}$.

The analytical data are in agreement with the literature.[4]

## 2.2 1,8-Bis(5-methyl-thiophen-2-yl)octa-1,7-diyne (2)

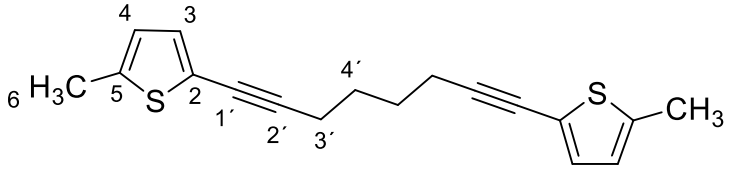


In a $N_2$-filled GB, a mixture of 2-methyl-5-iodothiophene (2.00 g, 8.93 mmol), $[PdCl_2(PPh_3)_2]$ (253 mg, 4 mol%, 360 μmol) and Cu(I)I (68.6 mg, 4 mol%, 360 μmol) in anhydrous, degassed TEA (5.00 mL) and anhydrous, degassed toluene (5.00 mL) was stirred at 22 °C. After addition of 1,7-octadiyne (450 mg, 4.24 mmol), the suspension was stirred at 80 °C for 8 h.

Then, the reaction was quenched with a sat. soln. of $NH_4Cl$ (1 x 50 mL). The aqueous layer was extracted with $Et_2O$ (3 x 100 mL) and the combined organic layers were washed with $H_2O$ (1 x 100 mL). The phases were separated, the organic phase was dried over $MgSO_4$ and filtered. The volatiles were removed *in vacuo*. The product was purified by column chromatography (gradient from 100% *n*-pentane to 1:5 DCM/*n*-pentane, $R_f$ = 0.44) to give a yellow-brownish oil, which crystallised at 5 °C (527 mg, 40%). M.P.: 50 °C; $^1$H NMR (500 MHz, $CDCl_3$): δ 6.92 (d, $^3J_{HH}$ = 3.5 Hz, 2H, H-3), 6.58 (d, $^3J_{HH}$ = 3.5 Hz, $^4J_{HH}$ = 1.1 Hz, 2H, H-4), 2.52 – 2.45 (m, 4H, H-3´), 2.44 (s, 6H, H-6), 1.77 – 1.72 (m, 4H, 4´) ppm; $^{13}$C{$^1$H} NMR (126 MHz, $CDCl_3$): δ 140.7 (C-5), 131.3 (C-3), 125.1 (C-4), 121.7 (C-2), 93.0 (C-2´), 74.5 (C-1´), 27.9 (C-3´), 19.4 (C-4´), 15.5 (C-6) ppm; IR (ATR): *ν* 2952 (w), 2932 (w), 2895 (w), 2866 (w), 2821 (w), 1751 (w), 1605 (w), 1538 (w), 1470 (m), 1457 (w), 1418 (m), 1333 (w), 1320 (w), 1306 (w), 1236 (w), 1187 (m), 1159 (m), 1045 (m), 992 (w), 966 (w), 898 (w), 888 (m), 875 (w), 801 (s), 758 (m), 732 (w), 675 (m) cm$^{-1}$; HR-MS (EI, $C_{18}H_{18}S_2$) calcd. 298.08444, found 298.08456 (R = 10000); MS (EI, 70 eV, direct inlet, 200 °C): *m*/*z* (% relative intensity) = 298 (100) $[M]^{+\cdot}$.

Rosenthal´s zirconocene (**3**) was reproduced according to the known procedure of Rosenthal et al.[5-6]

## 2.3 1,1',3,3'-Tetrakis(5-methylthiophen-2-yl)-4,4',5,5',6,6',7,7'-octahydro-2,2'-spirobi[benzo[*c*]stannole] (4)

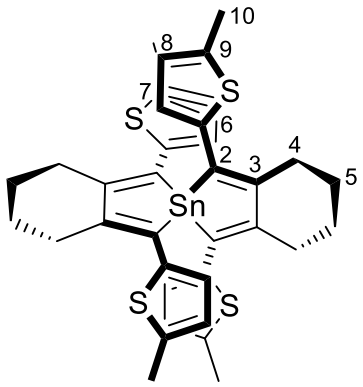


In a $N_2$-filled GB, 1,8-bis(5-methylthiophen-2-yl)octa-1,7-diyne (150 mg, 503 μmol) and Rosenthal´s zirconocene (237 mg, 503 μmol) were dissolved in anhydrous, degassed toluene (8 mL). The dark red solution was stirred at 22 °C for 18 h. Then, Cu(I)Cl (4.9 mg, 50 μmol) was added. At the Schlenk line, the reaction mixture was stirred at -78 °C and $SnCl_4$ (0.25 mL, 252 μmol, 1 M in heptanes) was added dropwise over the course of 1 min. The reaction was stirred at -78 °C for 1 h and then at 22 °C for 16 h. The reaction mixture was quenched with $H_2O$ (1 x 50 mL) and extracted with $Et_2O$ (3 x 50 mL). The combined organic layers were dried over $MgSO_4$, filtered and concentrated *in vacuo*. The crude product was purified by column chromatography (silica gel, gradient from 100% *n*-pentane to 100% DCM, $R_f$ = 0.14) and then crystallised from a sat. soln. of toluene to give orange-yellow crystals (50 mg, 28%). M.P.: the colour of the compound changed from orange-yellow to dark reddish-black at 232 °C and melted at 248 °C; $\lambda_{abs,\,max}$ ($CHCl_3$, ε = 31235 $L \cdot mol^{-1} \cdot cm^{-1}$) = 436 nm; $\lambda_{em,\,max}$ ($CHCl_3$) = 533 nm; $^1$H NMR (600 MHz, $CDCl_3$): δ 6.60 (d, $^3J_{HH}$ = 3.6 Hz, 2H, H-7), 6.52 (d, $^3J_{HH}$ = 3.6 Hz, $^4J_{HH}$ = 1.2 Hz, 2H, H-8), 2.95 – 2.82 (m, 4H, H-4), 2.40 (s, 6H, H-10), 1.86 – 1.78 (m, 4H, 5) ppm; $^{13}$C{$^1$H} NMR (151 MHz, $CDCl_3$): δ 147.1 (C-3, $^2J_{SnC}$ = 42.7 Hz), 143.1 (C-6, $^2J_{SnC}$ = 39.0 Hz), 140.6 (C-9), 129.9 (C-7, $^4J_{SnC}$ = 14.5 Hz), 129.3 (C-2, $^1J_{SnC}$ = 226.5, 217 Hz), 125.5 (C-8), 31.6 (C-4, $^3J_{SnC}$ = 31.2 Hz), 23.4 (C-5), 15.7 (C-10) ppm; $^{119}$Sn{$^1$H} NMR (224 MHz, $CDCl_3$): δ -36.0 ppm; IR (ATR): *ν* 3075 (w), 2946 (w), 2911 (w), 2851 (w), 2814 (w), 1524 (w), 1432 (w), 1415 (w), 1371 (w), 1358 (w), 1338 (w), 1250 (w), 1211 (m), 1158 (w), 1133 (w), 1088 (w), 1052 (w), 1021 (w), 992 (w), 922 (w), 901 (w), 863 (w), 822 (w), 788 (m), 738 (w), 713 (w), 661 (m) $cm^{-1}$; HR-MS (EI, $C_{18}H_{18}S_2$) calcd. 712.07195, found 712.07069 (R = 10000); MS (EI, 70 eV, direct inlet, 200 °C): *m*/*z* (% relative intensity) = 716 (100) $[M]^{+\cdot}$.

## 2.4 Monitoring of the Reaction of Spirostannole 4 with MeLi by NMR measurements – Lithium Pentaorganostannate 5[7-8]

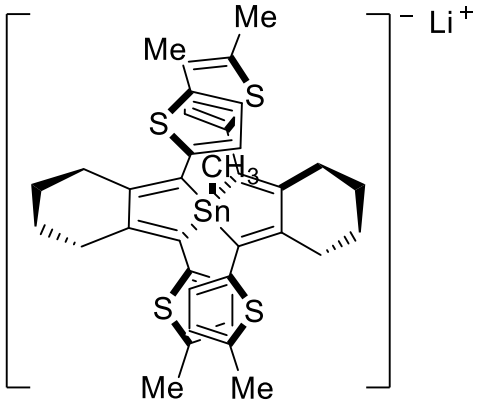


In an inert NMR tube, spirostannole **4** (5.8 mg, 8.1 μmol) was dissolved in anhydrous, degassed THF under an Ar atmosphere. At -78 °C, MeLi (1.6 M in $Et_2O$, 6 μL, 8.9 μmol) was added to this solution, the colour directly changed from orange-yellow to red. NMR spectra were recorded at -35 °C (this was the minimum temperature of the device) and then again at 25 °C. After finishing all measurements, the mixture was brownish-turbid yellow indicating the decomposition of the compound. $^{119}Sn\{^1H\}$ NMR (224 MHz, $CDCl_3$, 238.15 K): δ -211.2 ppm; $^7Li$ NMR (233 MHz, $CDCl_3$, 238.15 K): δ -0.4 ppm.

**Figure S1.** Spirostannole 4 in degassed, anhydrous THF at −78 °C in an inert NMR tube.

**Figure S2.** Spirostannole 4 with MeLi in degassed, anhydrous THF at −78 °C in an inert NMR tube.

# 3. Crystallography

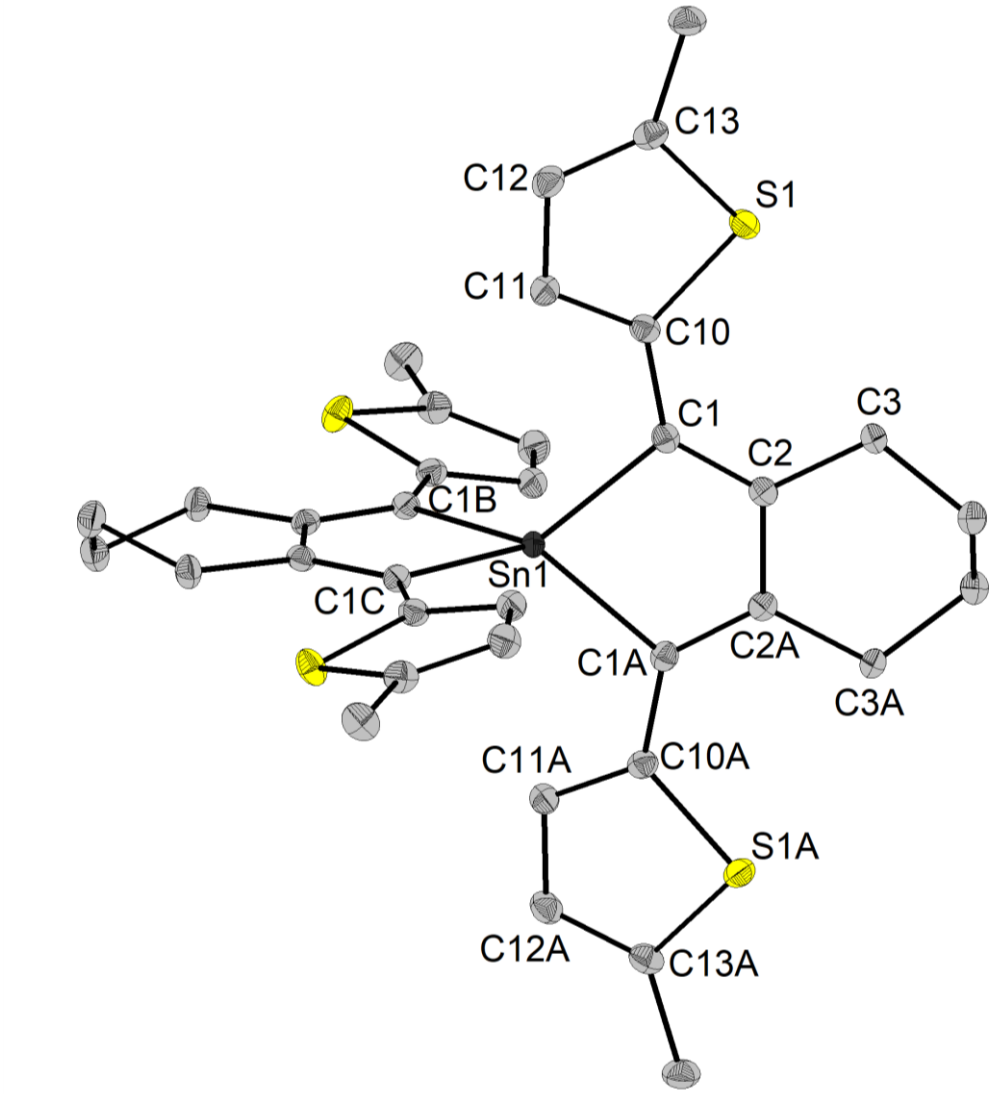


**Figure S3.** Molecular structure of spirostannole 4 showing 50% probability ellipsoids and the crystallographic numbering scheme. All hydrogen atoms are omitted for clarity.

**Table S3.** Crystal data and structure refinement for 4.

| **CCDC number** | **2027202** |
|---|---|
| Empirical formula | $C_{36}H_{36}S_4Sn$ |
| Formula weight | 715.58 |
| Temperature [K] | 100.0 |
| Crystal system | 'orthorhombic' |
| Space group (number) | *C*cce (68) |
| *a* [Å] | 14.5502(7) |
| *b* [Å] | 17.9138(9) |
| *c* [Å] | 11.6528(6) |
| *α* [Å] | 90 |
| β [Å] | 90 |
| γ [Å] | 90 |
| Volume [Å$^3$] | 3037.3(3) |
| Z | 4 |

| | |
|---|---|
| $\rho_{calc}$ [g/cm$^3$] | 1.565 |
| $\mu$ [mm$^{-1}$] | 1.142 |
| $F$(000) | 1464 |
| Crystal size [mm$^3$] | 0.2×0.2×0.1 |
| Crystal colour | orange |
| Crystal shape | plate |
| Radiation | Mo$K_\alpha$ ($\lambda$=0.71073 Å) |
| 2θ range [°] | 5.02 to 56.99 (0.74 Å) |
| Index ranges | -19 ≤ h ≤ 19<br>-24 ≤ k ≤ 23<br>-13 ≤ l ≤ 15 |
| Reflections collected | 14689 |
| Independent reflections | 1930<br>$R_{int}$ = 0.0387<br>$R_{sigma}$ = 0.0258 |
| Completeness to θ = 25.242° | 99.8 % |
| Data / Restraints / Parameters | 1930/0/95 |
| Goodness-of-fit on $F^2$ | 1.088 |
| Final $R$ indexes | $R_1$ = 0.0285 |
| [$I$≥2σ($I$)] | w$R_2$ = 0.0703 |
| Final $R$ indexes | $R_1$ = 0.0360 |
| [all data] | w$R_2$ = 0.0743 |
| Largest peak/hole [eÅ$^3$] | 1.01/-0.47 |

**Table S4.** Selected bond lengths and angles for 4.

| | **Length [Å]** |
|---|---|
| Sn1–C1$^B$ | 2.136(2) |
| Sn1–C1$^A$ | 2.136(2) |
| Sn1–C1 | 2.136(2) |
| Sn1–C1$^C$ | 2.136(2) |
| S1–C10 | 1.755(2) |
| S1–C13 | 1.725(2) |
| C1–C2 | 1.357(3) |
| C1–C10 | 1.452(3) |
| C11–C10 | 1.373(3) |
| C11–C12 | 1.419(3) |
| C2–C2$^A$ | 1.507(4) |
| C2–C3 | 1.520(3) |
| C3–C4 | 1.524(3) |
| C12–C13 | 1.364(3) |
| C4–C4$^A$ | 1.510(5) |
| C14–C13 | 1.510(3) |
| | **Angle [°]** |
| C1$^B$–Sn1–C1$^C$ | 83.5(2) |
| C1$^A$–Sn1–C1 | 83.5(2) |
| C1$^B$–Sn1–C1 | 126.0(2) |
| C1$^B$–Sn1–C1$^A$ | 121.6(2) |
| C1$^C$–Sn1–C1$^A$ | 126.0(2) |
| C1$^C$–Sn1–C1 | 121.6(2) |
| C13–S1–C10 | 93.2(2) |
| C2–C1–Sn1 | 108.6(2) |
| C2–C1–C10 | 129.7(3) |
| C10–C1–Sn1 | 121.6(2) |
| C10–C11–C12 | 114.5(2) |
| C1–C2–C2$^A$ | 119.5(2) |

| | |
|---|---|
| C1–C2–C3 | 121.5(2) |
| C2$^{A}$–C2–C3 | 118.9(2) |
| C2–C3–C4 | 115.1(2) |
| C1–C10–S1 | 125.5(3) |
| C11–C10–S1 | 108.4(2) |
| C11–C10–C1 | 126.0(2) |
| C13–C12–C11 | 113.4(2) |
| C4$^{A}$–C4–C3 | 109.6(3) |
| C12–C13–S1 | 110.3(3) |
| C12–C13–C14 | 129.2(2) |
| C14–C13–S1 | 120.4(2) |

Symmetry transformations used to generate equivalent atoms: A: X, 0.5-Y, 0.5-Z; B: 1-X, Y, 0.5-Z; C: 1-X, 0.5-Y, Z;.

**Table S5.** Selected torsion angles for 4.

| | **Torsion Angle [°]** |
|---|---|
| Sn1–C1–C2–C2$^{A}$ | 1.8(3) |
| Sn1–C1–C2–C3 | -178.4(2) |
| Sn1–C1–C10–S1 | -167.3(2) |
| Sn1–C1–C10–C11 | 13.7(3) |
| C1–C2–C3–C4 | 165.2(2) |
| C11–C12–C13–S1 | -0.2(3) |
| C11–C12–C13–C14 | 179.2(2) |
| C2–C1–C10–S1 | 15.7(3) |
| C2–C1–C10–C11 | -163.3(2) |
| C2$^{A}$–C2–C3–C4 | -15.1(3) |
| C2–C3–C4–C4$^{A}$ | 49.0(3) |
| C10–S1–C13–C12 | -0.4(3) |
| C10–S1–C13–C14 | -179.9(3) |
| C10–C1–C2–C2$^{A}$ | 179.1(2) |
| C10–C1–C2–C3 | -1.1(4) |
| C10–C11–C12–C13 | 1.0(3) |
| C12–C11–C10–S1 | -1.3(2) |
| C12–C11–C10–C1 | 177.8(2) |
| C13–S1–C10–C1 | -178.1(2) |
| C13–S1–C10–C11 | 1.0(2) |

Symmetry transformations used to generate equivalent atoms: A: X, 0.5-Y, 0.5-Z;.

# 4. DFT and TD-DFT Calculations

Optimised equilibrium geometries were calculated on a DFT level with the Gaussian 16, revision A.03[9] quantum software package for a single molecule in the gas phase using the PBE1PBE/6-311++G(2d,2p)[10-15] level of theory including empirical dispersion corrections according to Grimme's D3[16-17] method involving Becke-Johnson damping (GD3BJ). For the Sn atom, we employed the Stuttgart/Dresden (SDD) pseudo potential.[18-19] The orbital energies of HOMO and LUMO and their energy differences were calculated for these optimised molecules. Frequency analyses were performed in all cases to confirm the absence of imaginary frequencies and thus prove that the obtained geometries corresponded to minima on the potential energy surface. The isodensity value for the molecular orbital isosurface representations was set to 0.02 a.u. in all cases. Absorption data was calculated using time-dependent DFT (TD-DFT) level on the optimised ground state geometries with the same functional and basis set as described above, i.e., TD-PBE1PBE-GD3BJ/6-311++G(2d,2p)//PBE1PBE-GD3BJ/6-311++G(2d,2p) employing SDD pseudo potentials for Sn.[10-19]

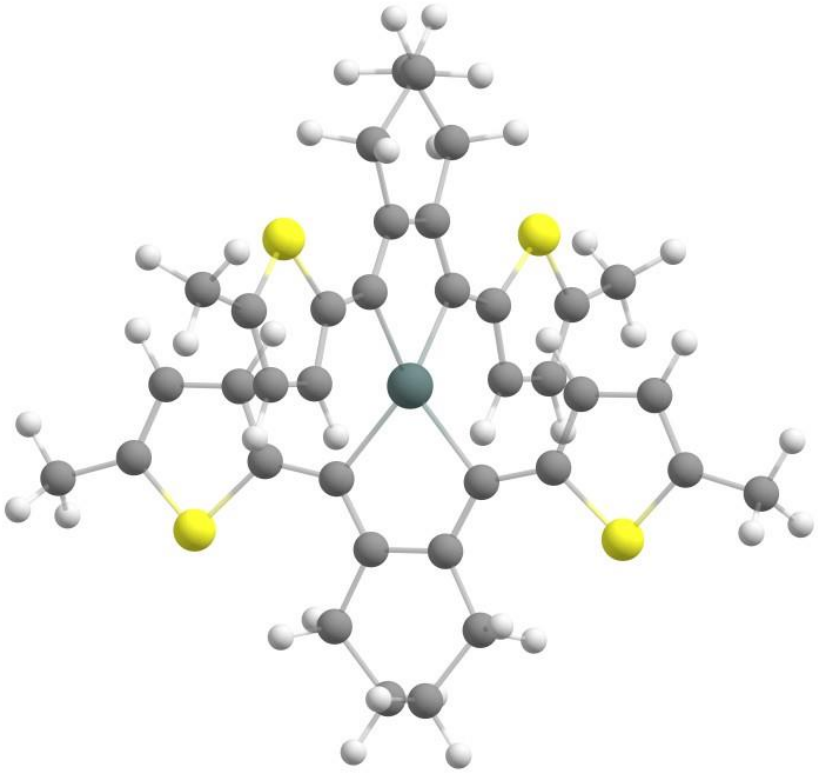

**Figure S4.** Optimised geometry of spirostannole **4**.

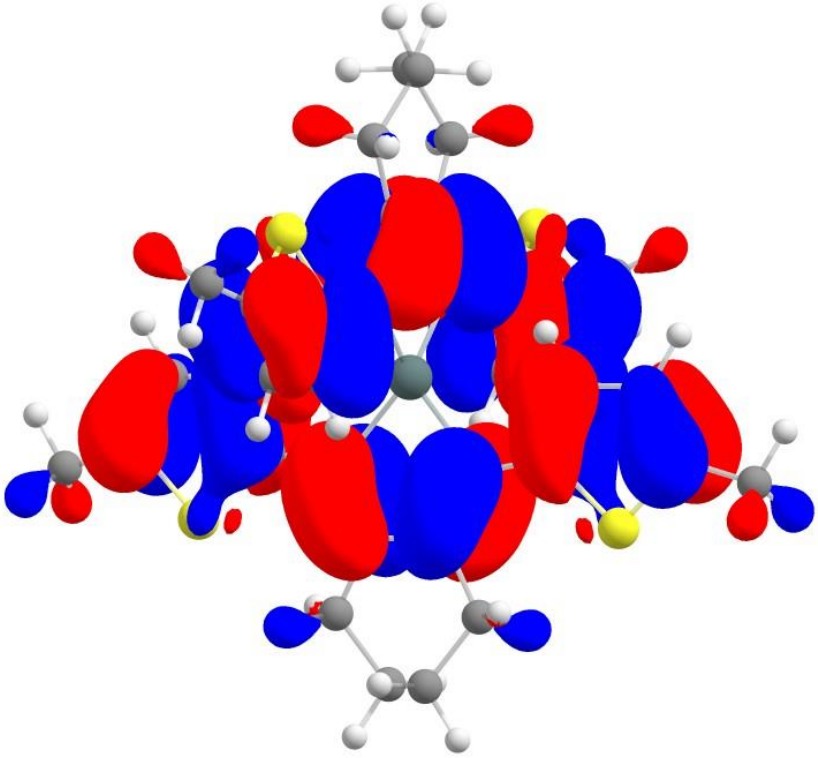

**Figure S5.** HOMO 1 of spirostannole 4.

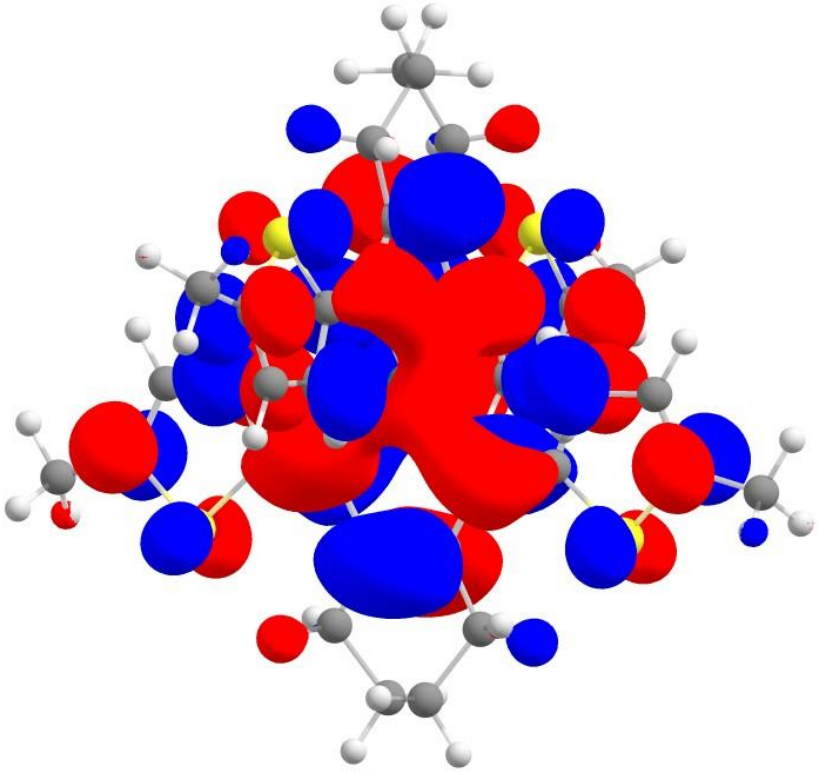

**Figure S6.** LUMO 1 of spirostannole 4.

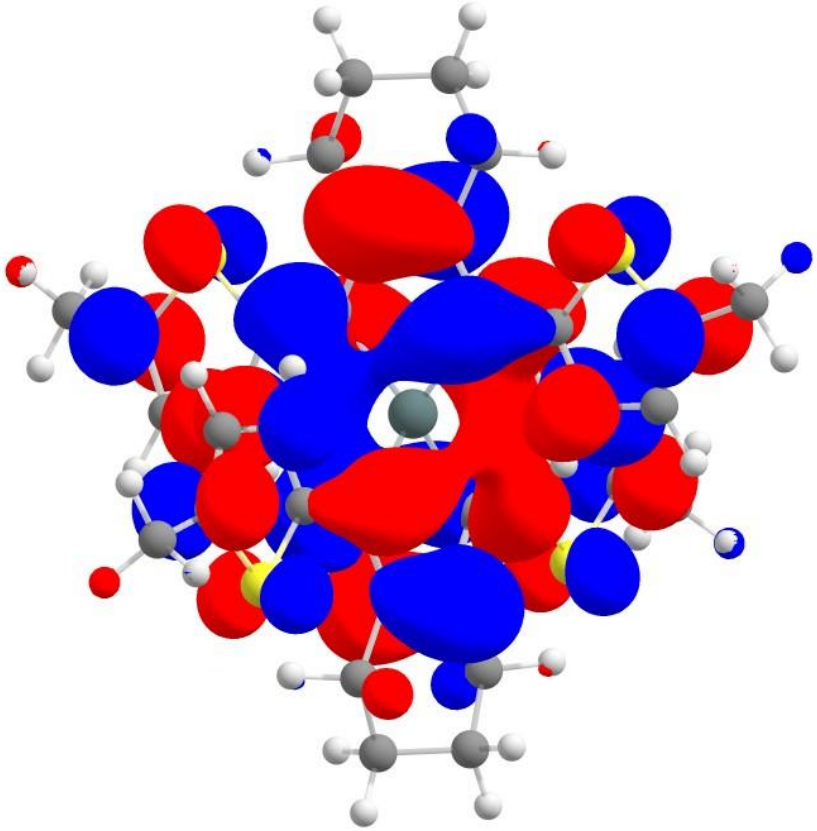

**Figure S7.** LUMO 1 of spirostannole 4, other viewing direction.

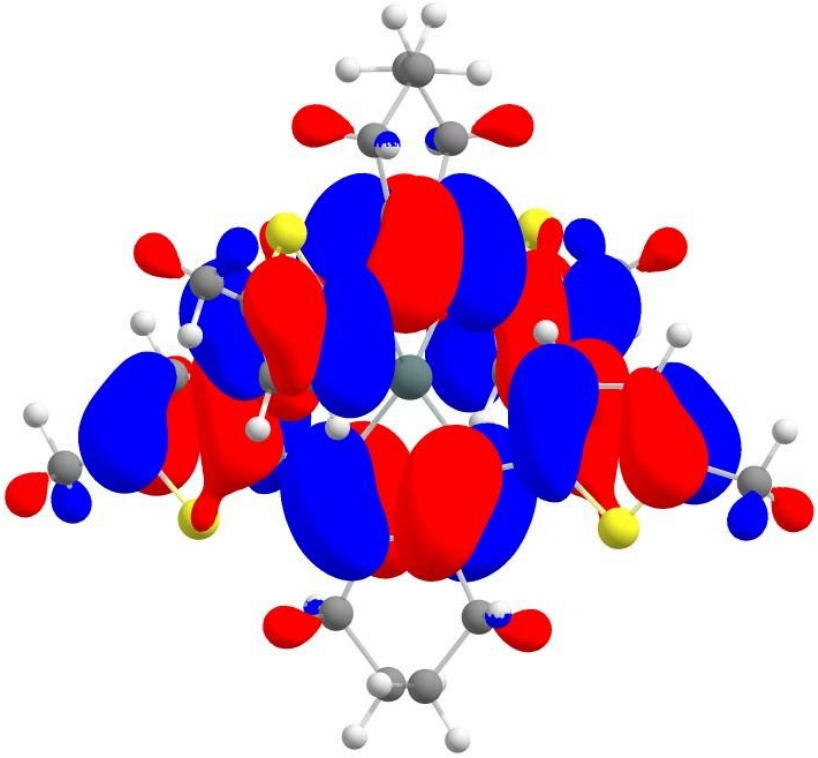

**Figure S8.** HOMO 2 of spirostannole 4.

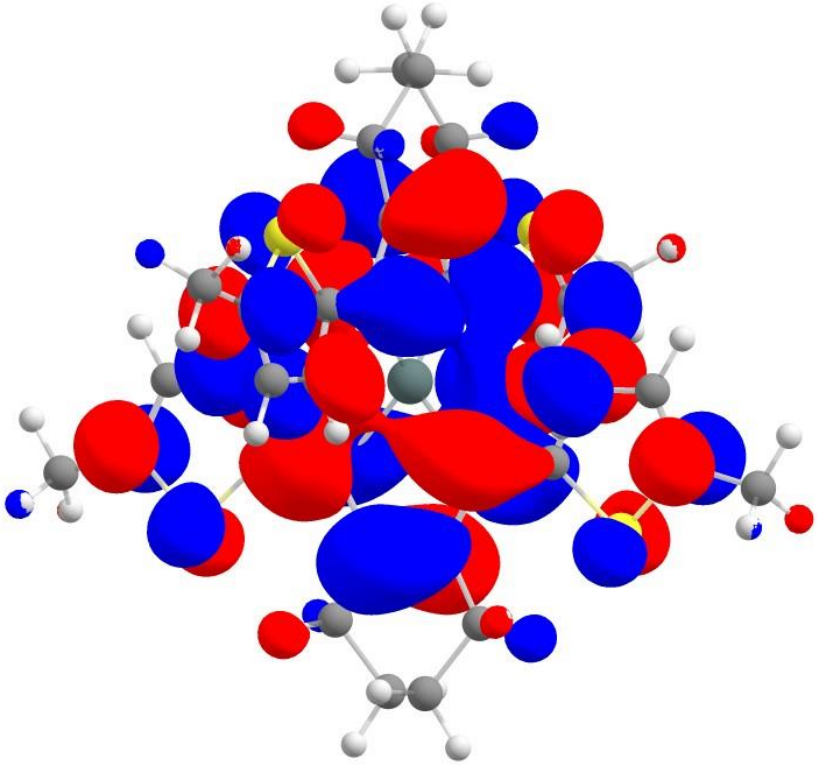

**Figure S9.** LUMO 2 of spirostannole 4.

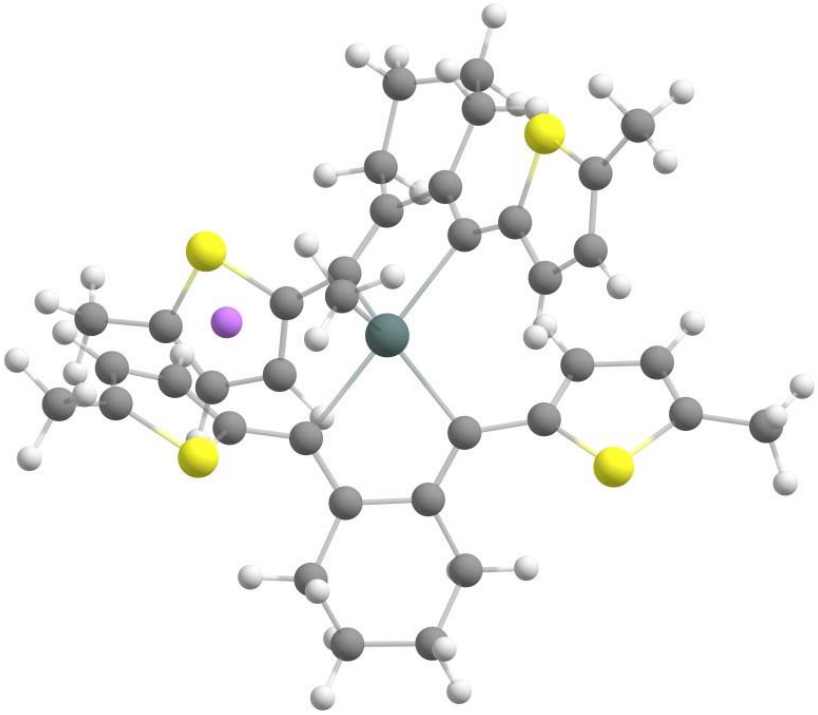

**Figure S10.** Optimised geometry of lithium pentaorganostannate 5.

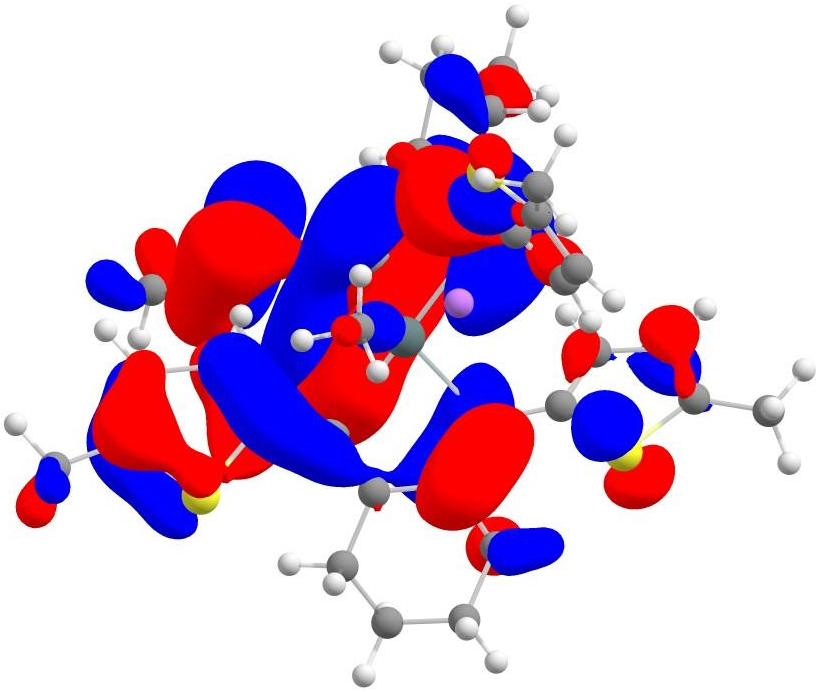

**Figure S11.** HOMO-4 of lithium pentaorganostannate 5.

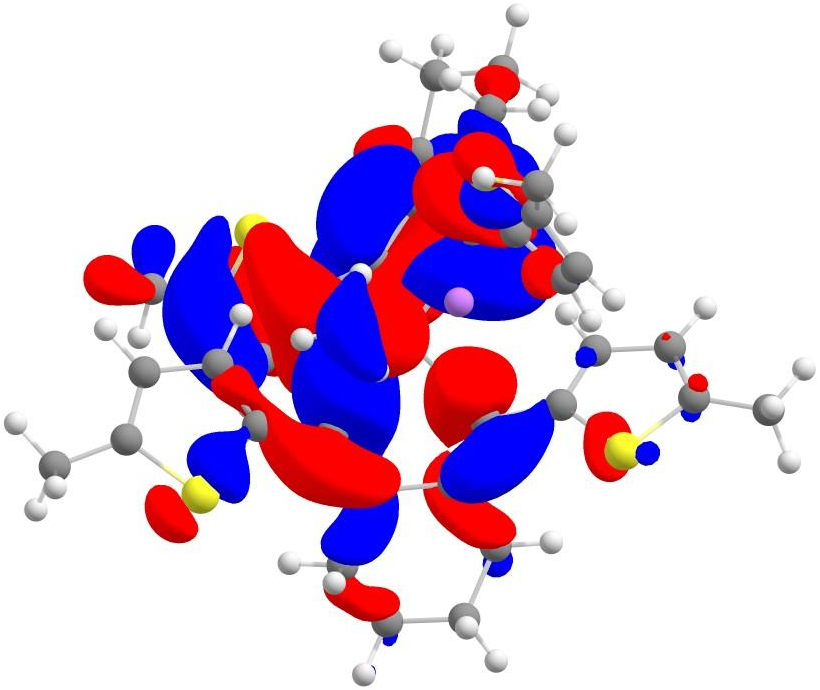

**Figure S12.** HOMO-2 of lithium pentaorganostannate 5.

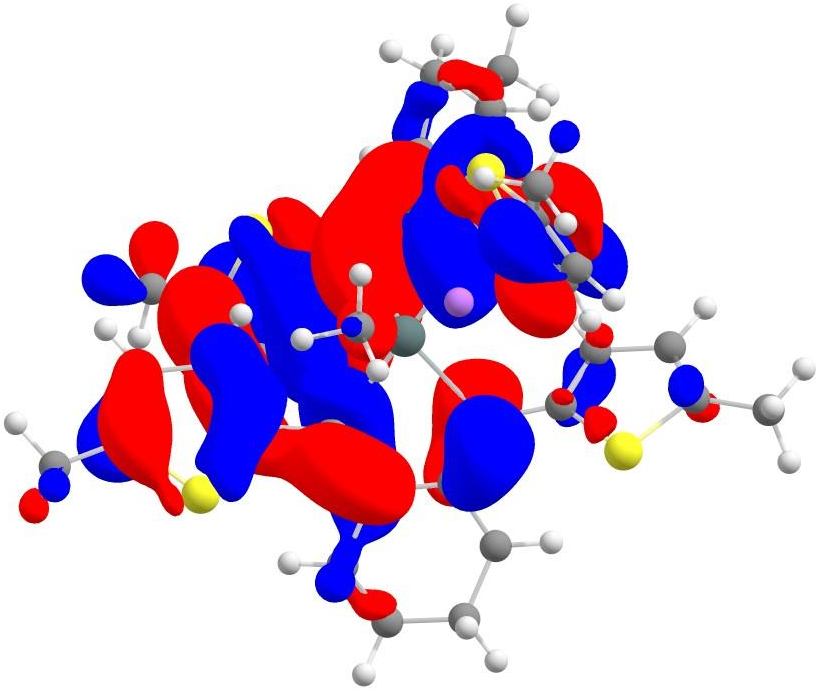

**Figure S13.** HOMO-1 of lithium pentaorganostannate 5.

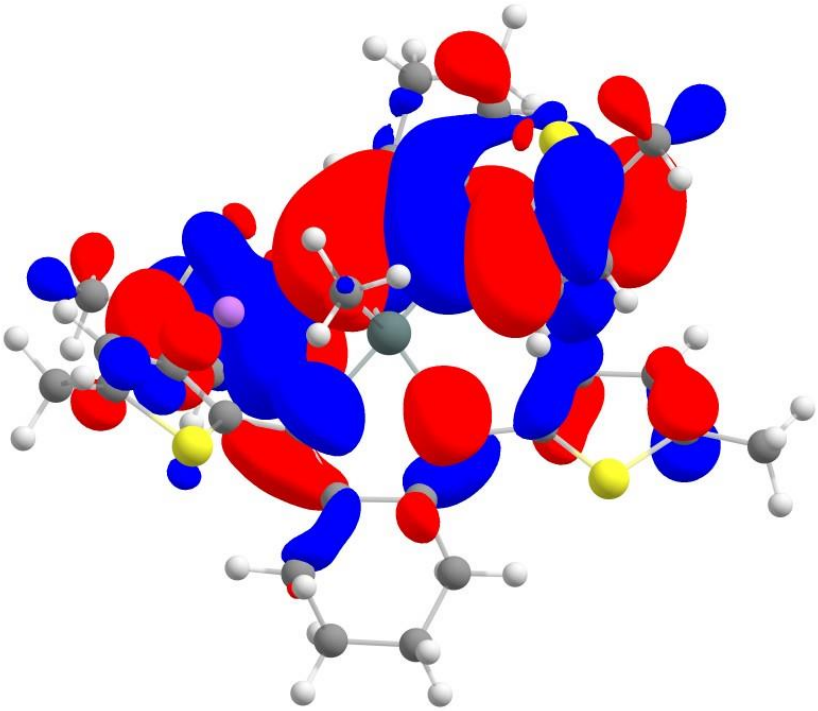

**Figure S14.** HOMO of lithium pentaorganostannate 5.

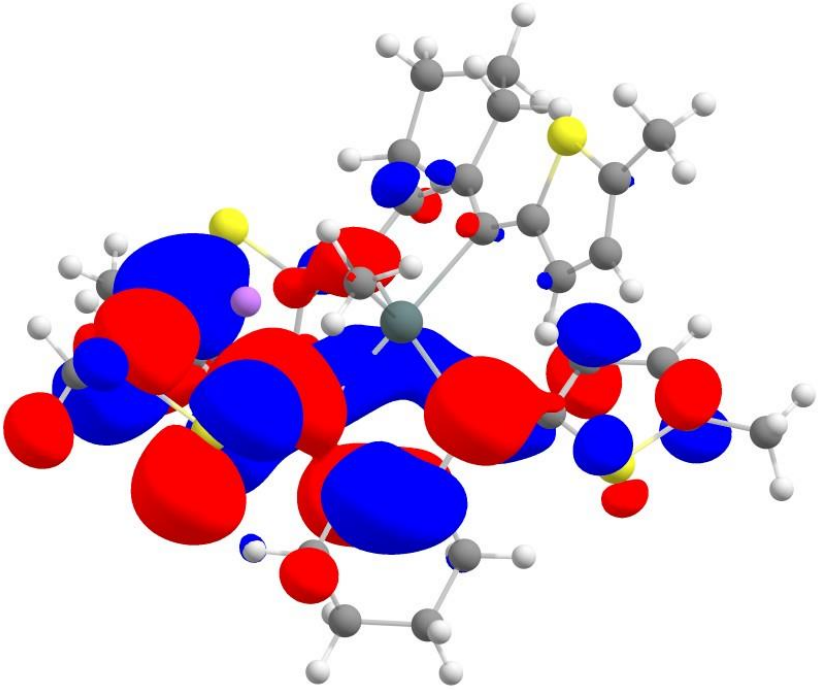

**Figure S15.** LUMO of lithium pentaorganostannate 5.

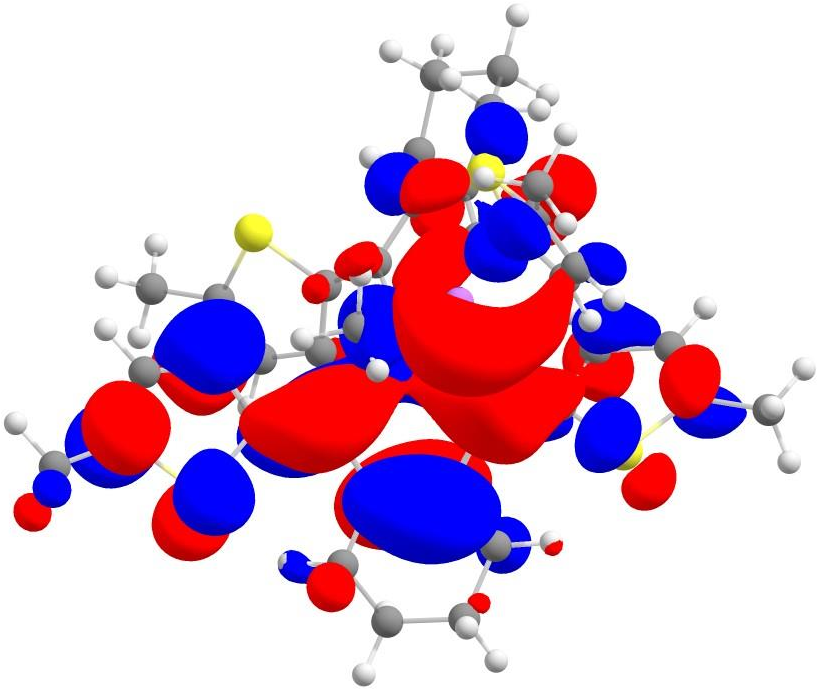

**Figure S16.** LUMO+1 of lithium pentaorganostannate 5.

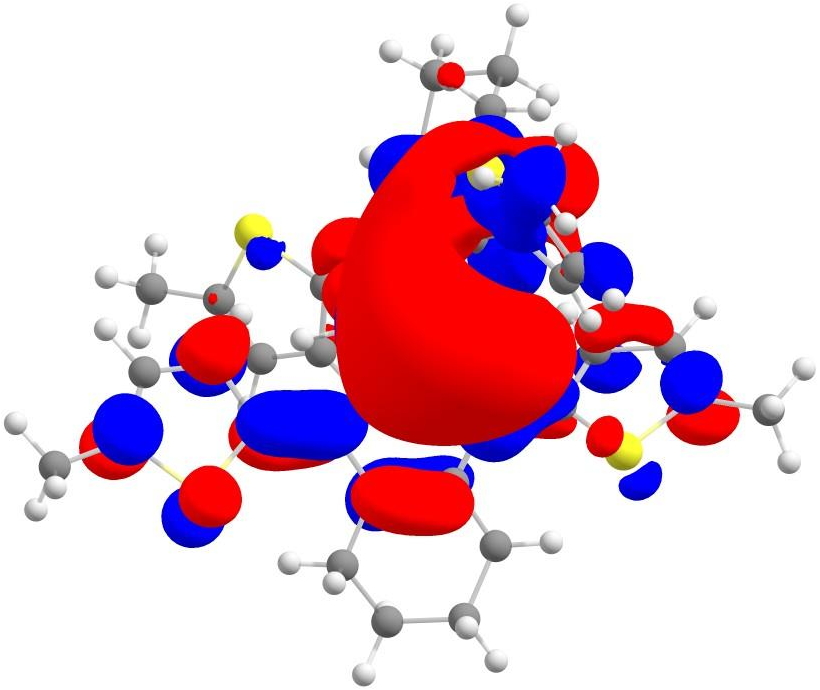

**Figure S17.** LUMO+2 of lithium pentaorganostannate 5.

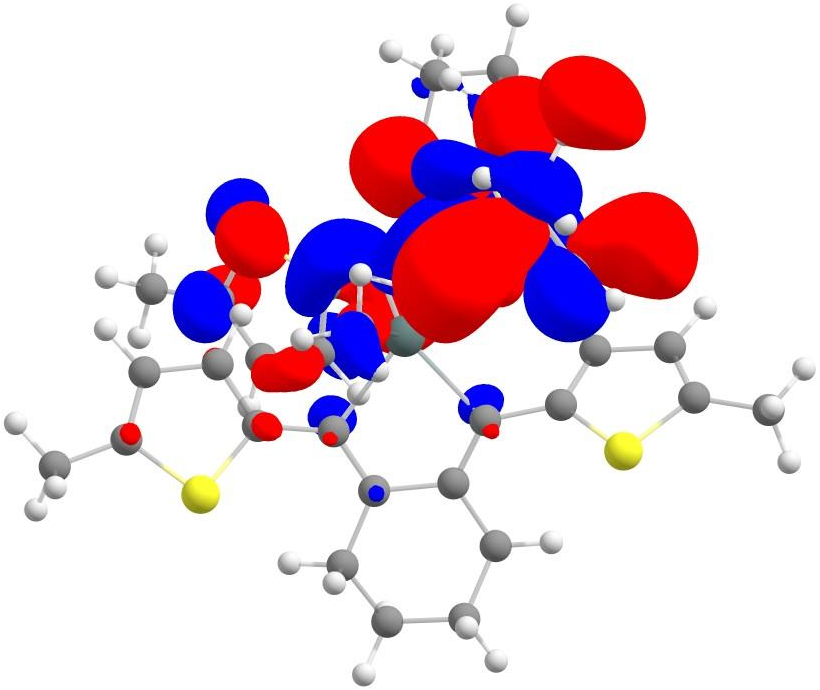

**Figure S18.** LUMO+3 of lithium pentaorganostannate 5.

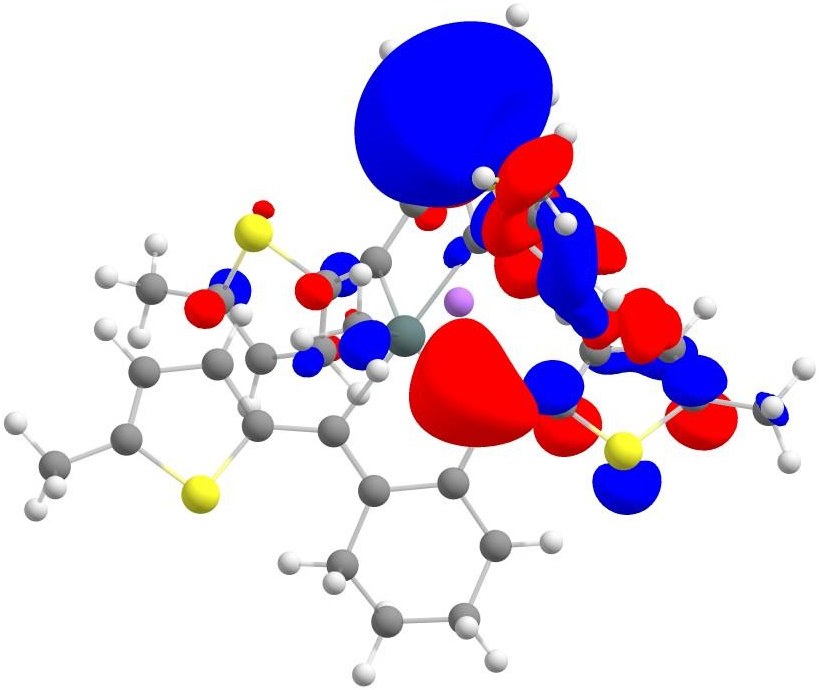

**Figure S19.** LUMO+4 of lithium pentaorganostannate 5.

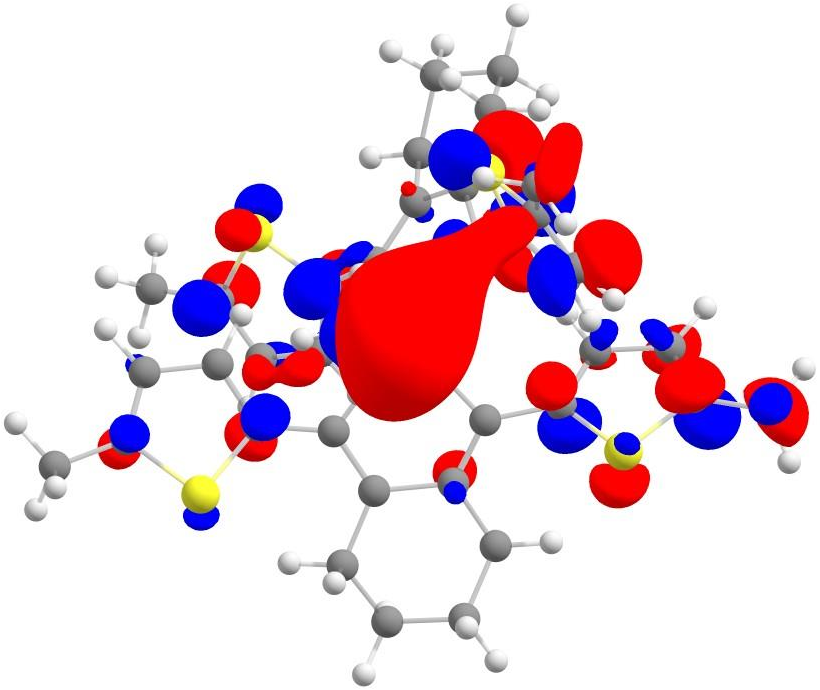

**Figure S20.** LUMO+5 of lithium pentaorganostannate 5.

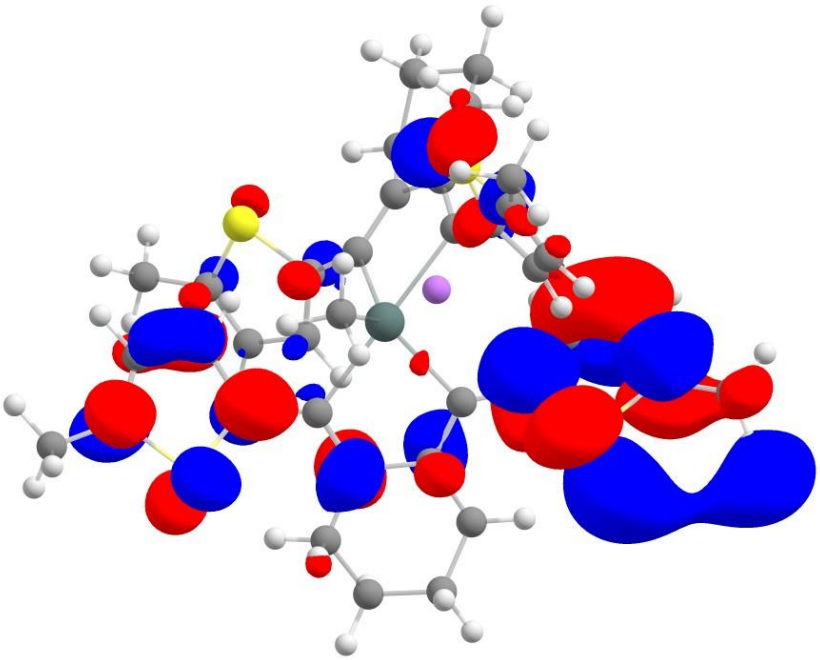

**Figure S21.** LUMO+7 of lithium pentaorganostannate 5.

# 4. Optical Properties and Cyclic Voltammetry Measurements

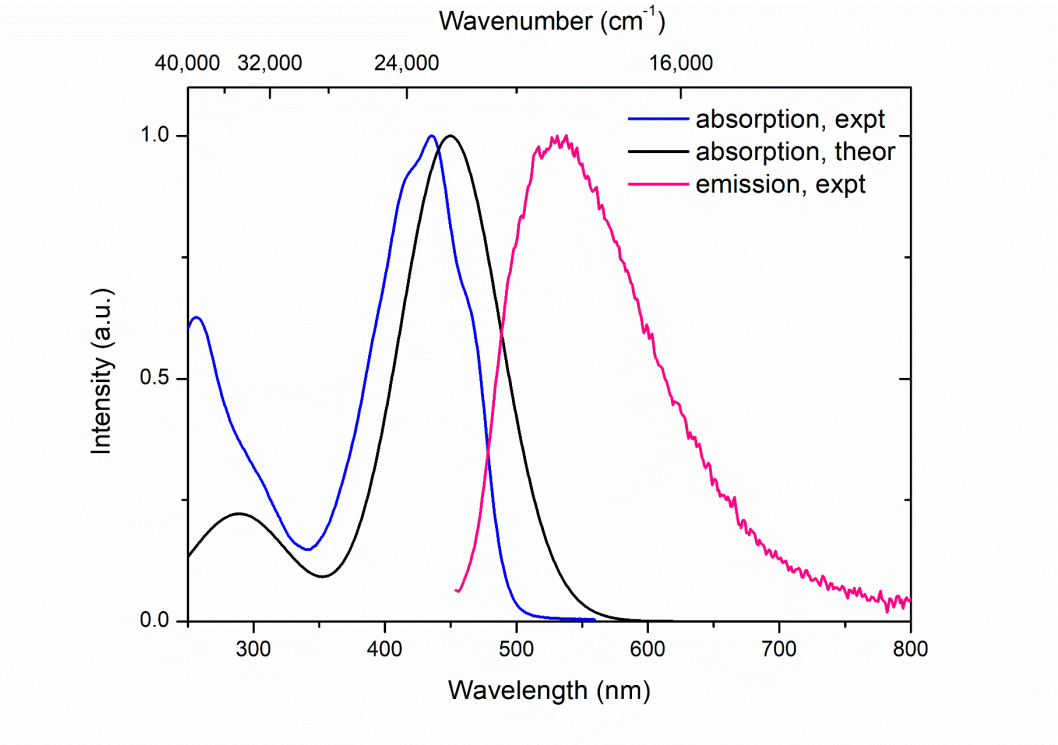


**Figure S22.** Normalised absorption and emission spectra of stannole 4 in chloroform ($c = 10^{-5}$ mol $L^{-1}$) and normalised theoretical absorption spectrum. The emission was monitored by excitation at 445 nm.

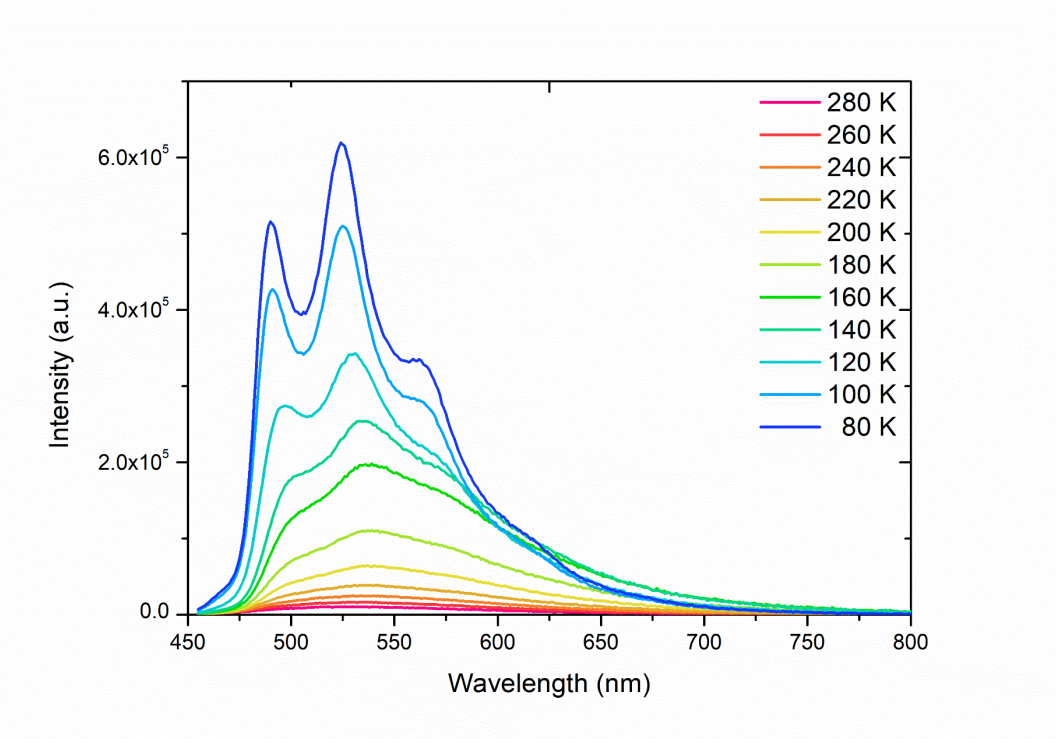

**Figure S23.** Temperature dependent emission spectra of stannole **4** in 2-methyltetrahydrofuran (c = $10^{-5}$ mol $L^{-1}$) during heating from 80 K to 280 K with excitation at 445 nm.

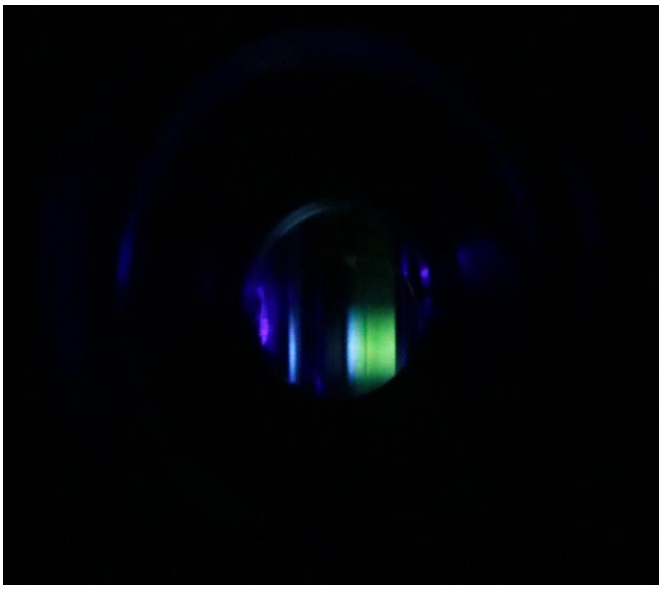

**Figure S24.** Irradiated sample of stannole **4** in 2-methyltetrahydrofuran (c = $10^{-5}$ mol $L^{-1}$) at 80 K with excitation at 445 nm.

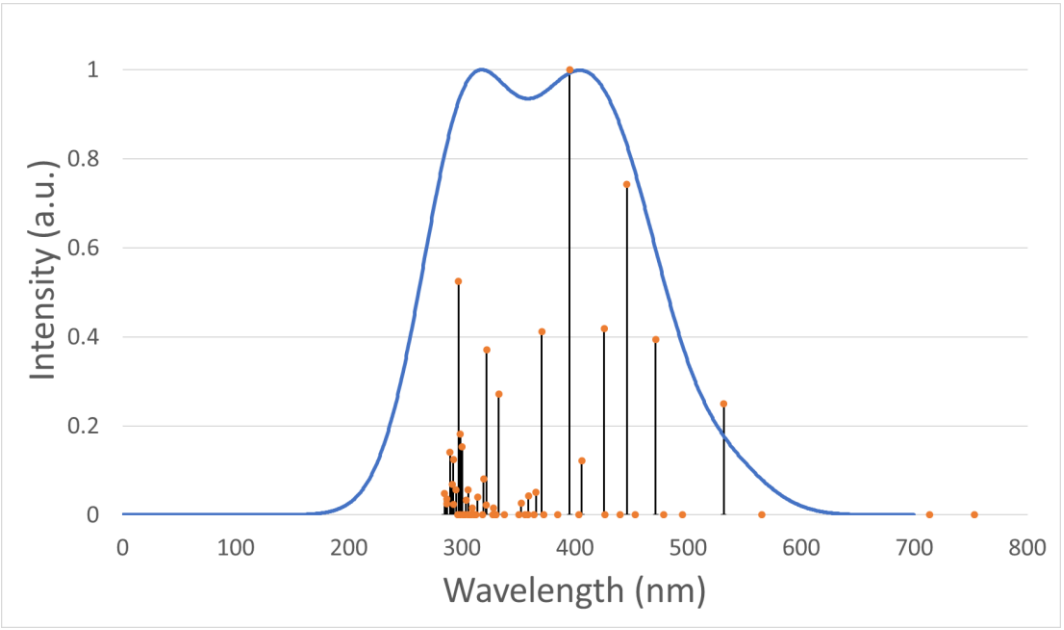


**Figure S25.** Theoretical absorption spectrum of lithium pentaorganostannate 5 with all transitions.

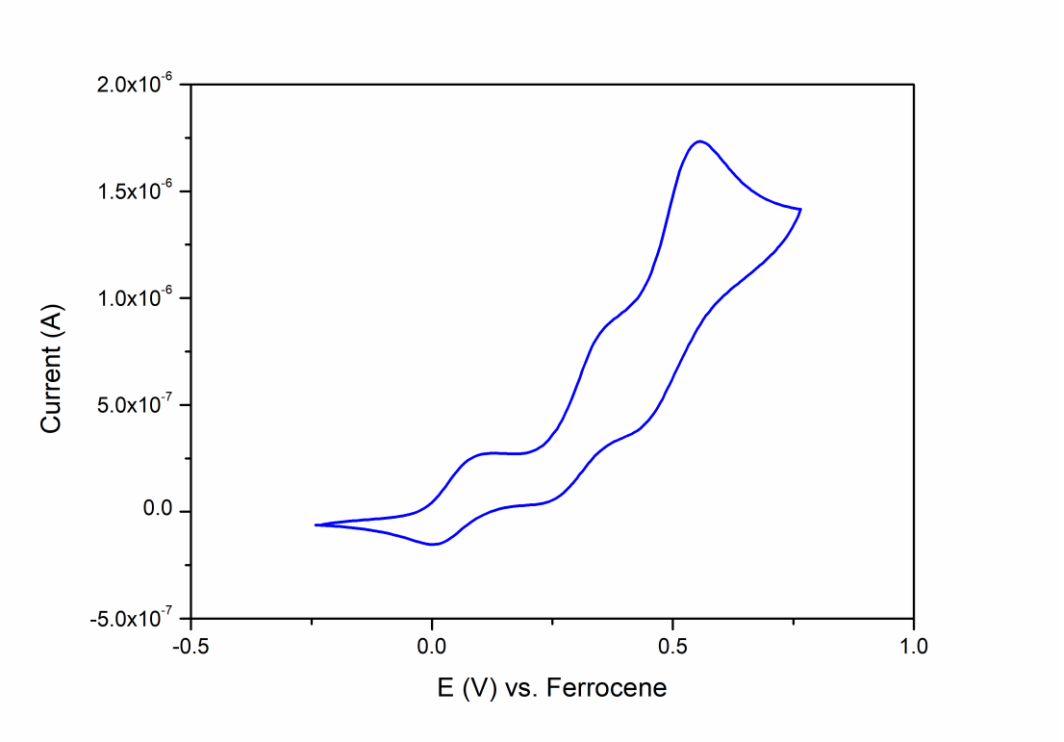


**Figure S26.** Cyclic voltammetry measurement of spirostannole **4** in DCM with TBA[$PF_6$] as conducting salt at a scan rate of 0.2 V/s.

**Table S6.** Significant absorption wavelengths for stannole 5 with involved transitions based on TD-DFT calculations.

| Absorption wavelength | Involved transitions | CI expansion coefficients |
|---|---|---|
| 532 nm | HOMO→LUMO | 0.10638 |
| | HOMO-2→LUMO | 0.68049 |
| 471 nm | HOMO→LUMO+1 HOMO→LUMO | 0.18927 |
| | HOMO-1→LUMO | 0.62113 |
| | HOMO-2→LUMO | -0.15123 |
| | | 0.15995 |
| 446 nm | HOMO→LUMO+1 | -0.17229 |
| | HOMO-1→LUMO+1 | 0.11038 |
| | HOMO-1→LUMO | -0.12018 |
| | HOMO-2→LUMO+1 | 0.14520 |
| | HOMO-2→LUMO | 0.63128 |
| 395 nm | HOMO→LUMO+2 HOMO→LUMO+1 | -0.16771 |
| | HOMO-1→LUMO+1 | 0.60320 |
| | HOMO-2→LUMO | -0.16285 |
| | | 0.22500 |
| 297 nm | HOMO-1→LUMO+7 | -0.10885 |
| | HOMO-1→LUMO+5 | 0.15864 |
| | HOMO-1→LUMO+4 | 0.54554 |
| | HOMO-2→LUMO+3 | 0.14677 |
| | HOMO-2→LUMO+2 | -0.15580 |
| | HOMO-4→LUMO+2 | 0.20805 |

# 5. NMR Spectra

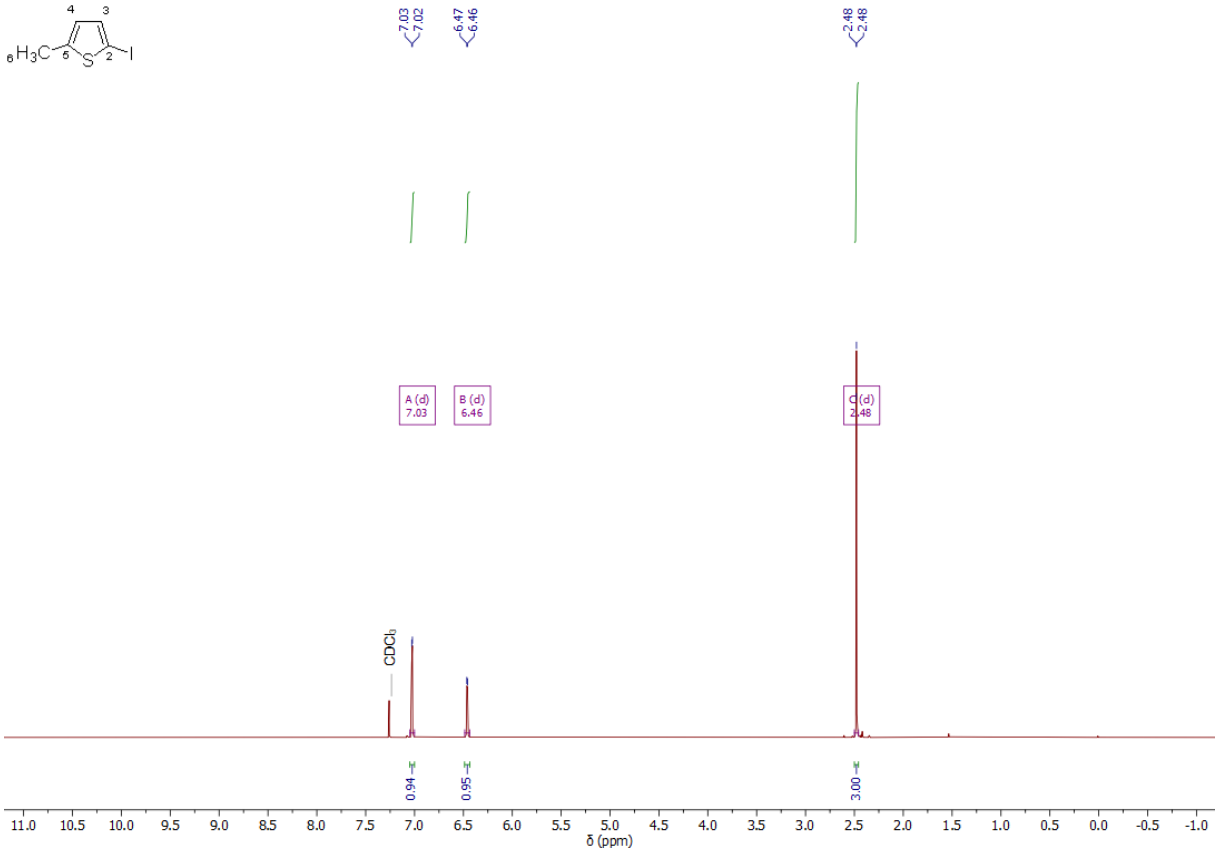


**Figure S27.** $^{1}$H NMR (500 MHz) spectrum of 1 in $CDCl_3$.

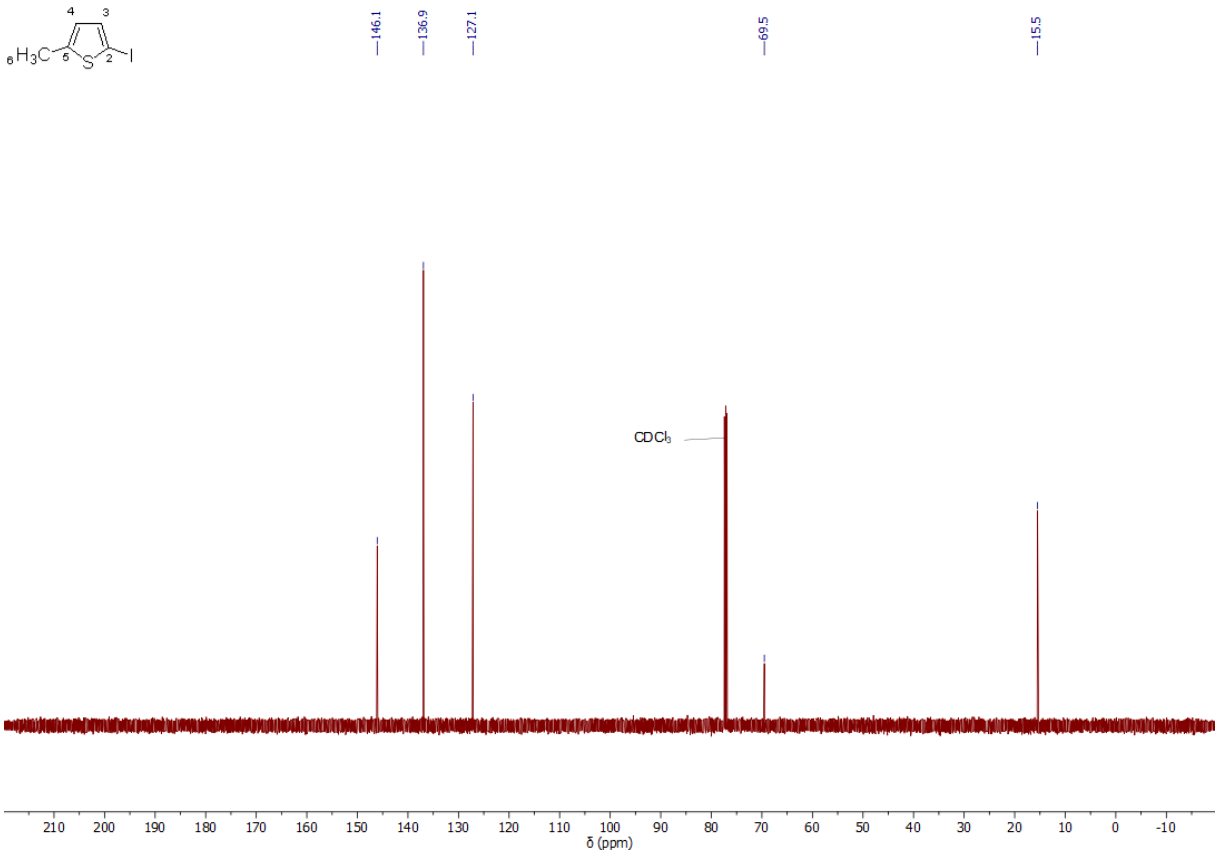


**Figure S28.** $^{13}C\{^{1}H\}$ NMR (126 MHz) spectrum of 1 in $CDCl_3$.

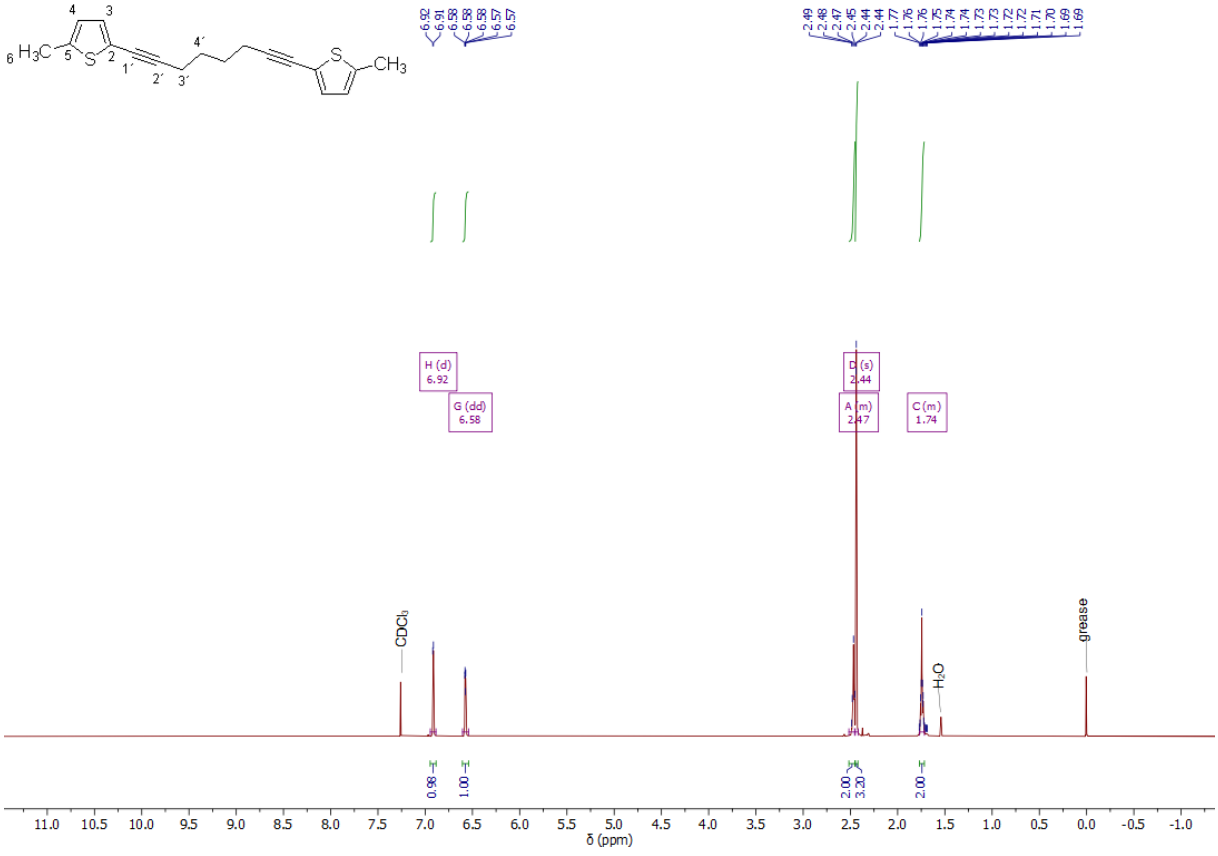


**Figure S29.** $^{1}H$ NMR (500 MHz) spectrum of 2 in $CDCl_3$.

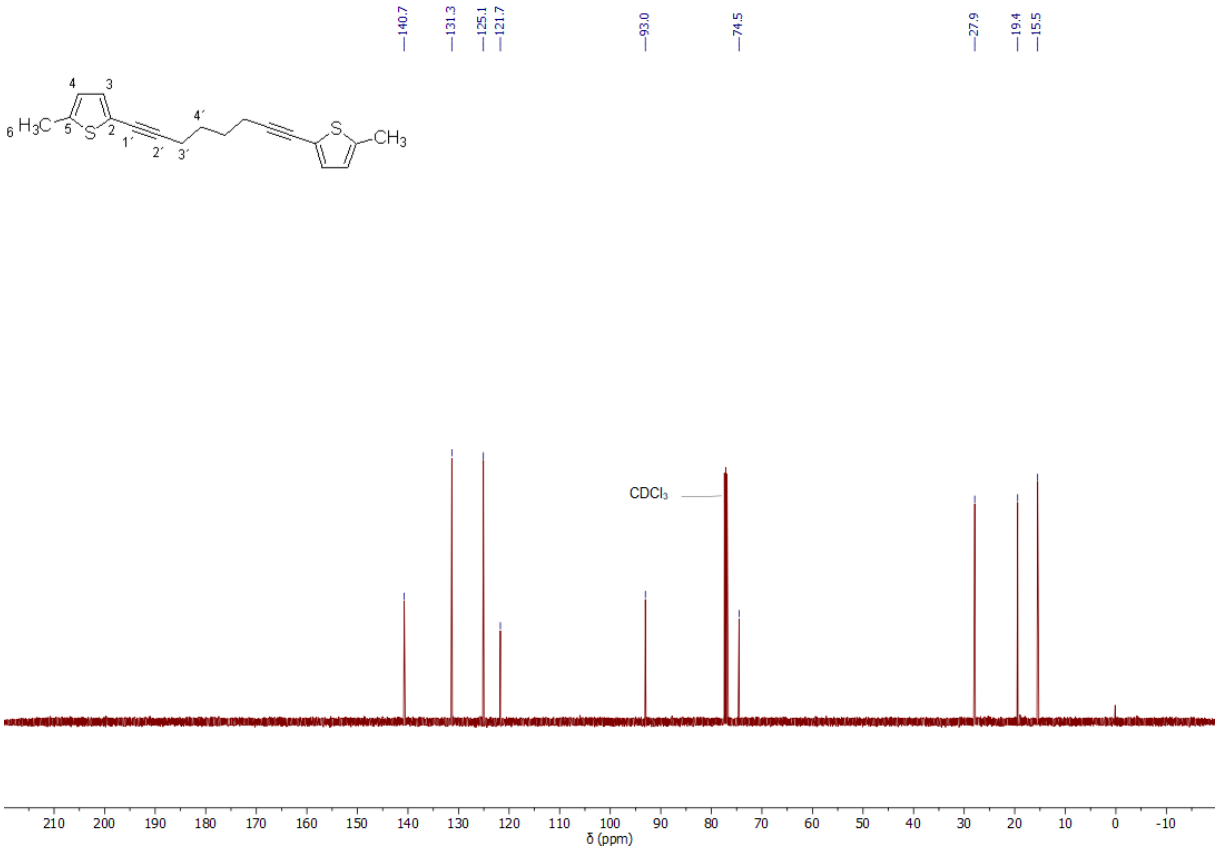


**Figure S30.** $^{13}C\{^{1}H\}$ NMR (126 MHz) spectrum of 2 in $CDCl_3$.

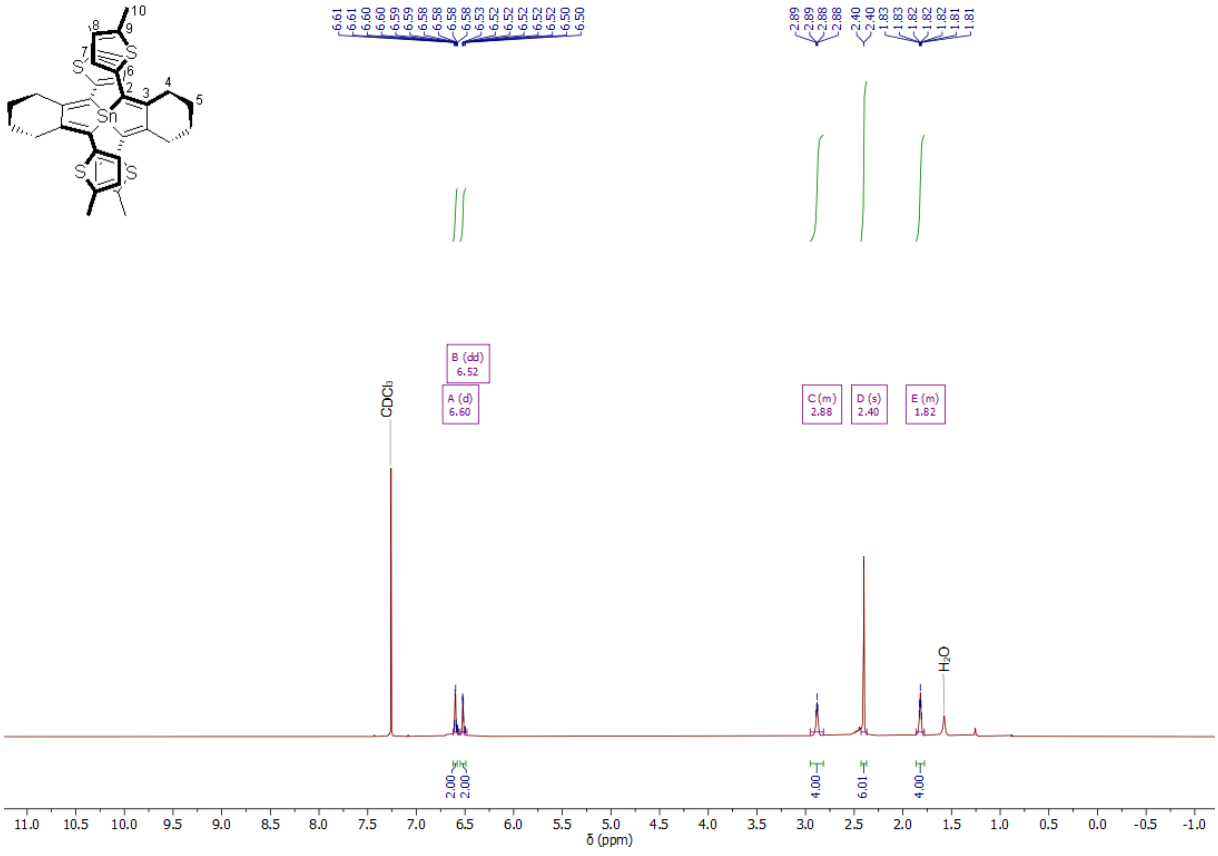


**Figure S31.** $^{1}H$ NMR (600 MHz) spectrum of 4 in $CDCl_3$.

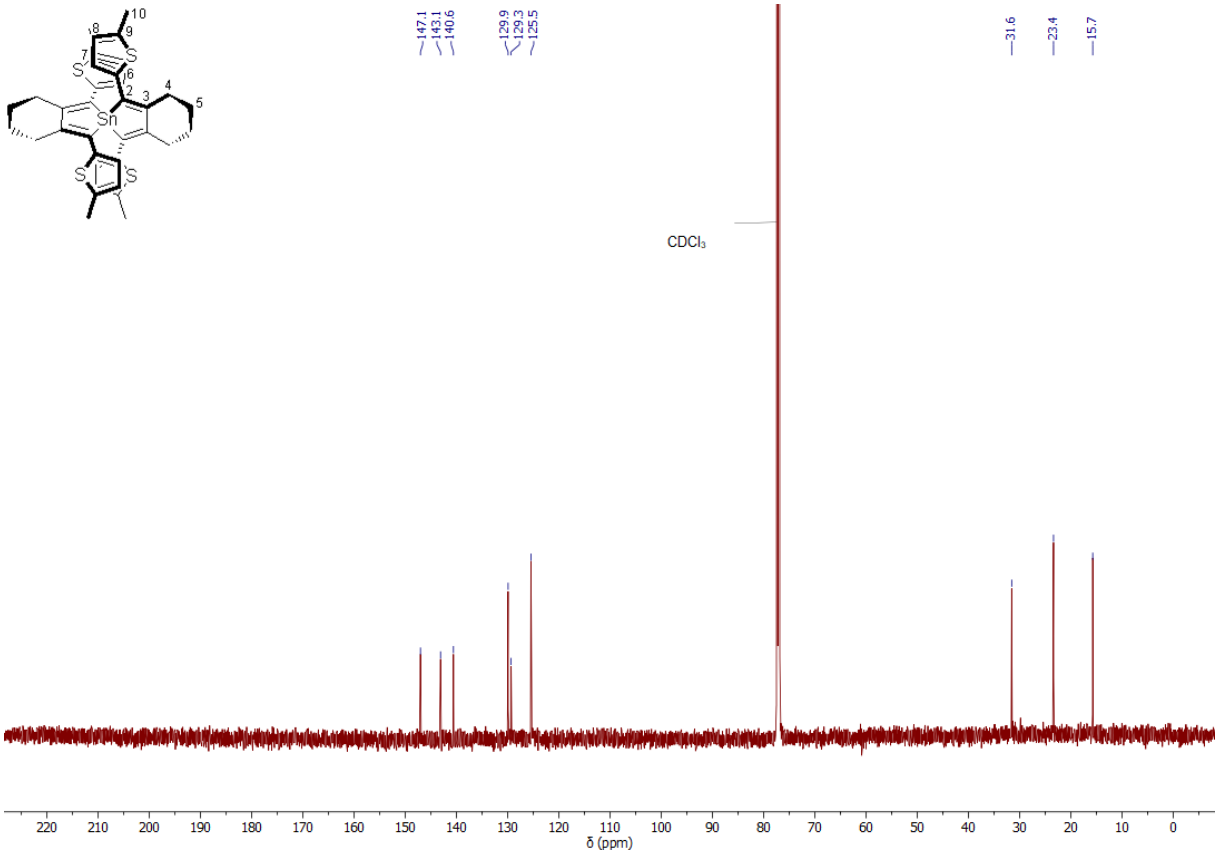


**Figure S32.** $^{13}C\{^{1}H\}$ NMR (151 MHz) spectrum of 4 in $CDCl_3$.

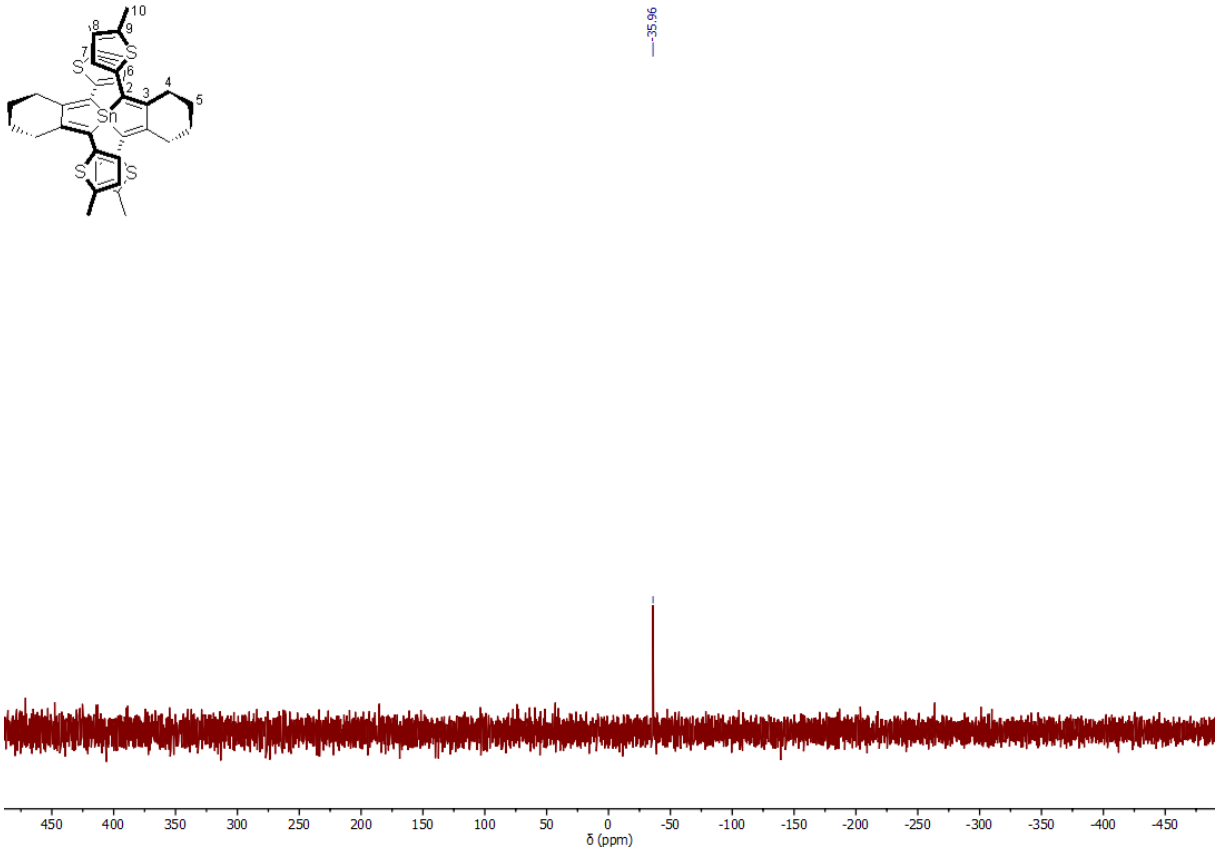


**Figure S33.** $^{119}Sn\{^{1}H\}$ NMR (224 MHz) spectrum of 4 in $CDCl_3$.

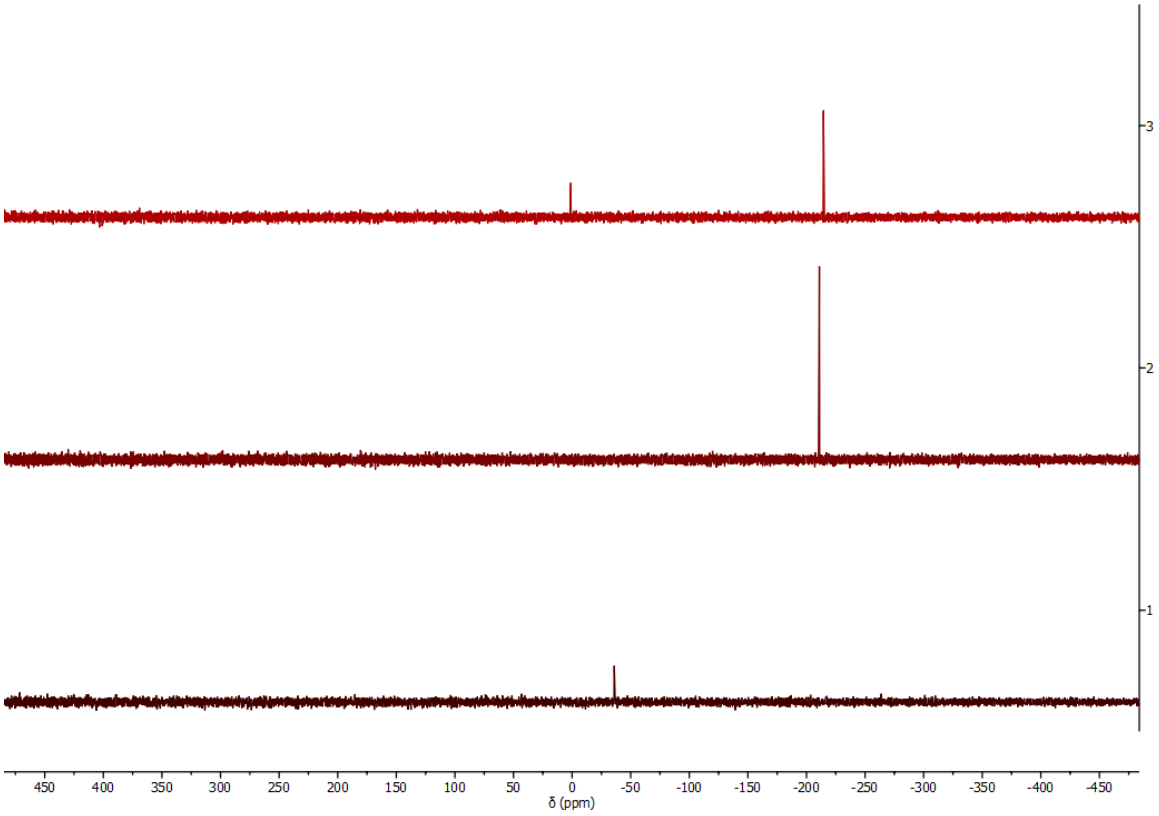


**Figure S34.** $^{119}Sn\{^{1}H\}$ NMR (224 MHz) spectrum of 4 (-36.0 ppm, bottom), 5 (-211.0 ppm, middle, -35 °C) and decomposition/ 5 (1.1 ppm and -211.0 ppm, above, 25 °C).

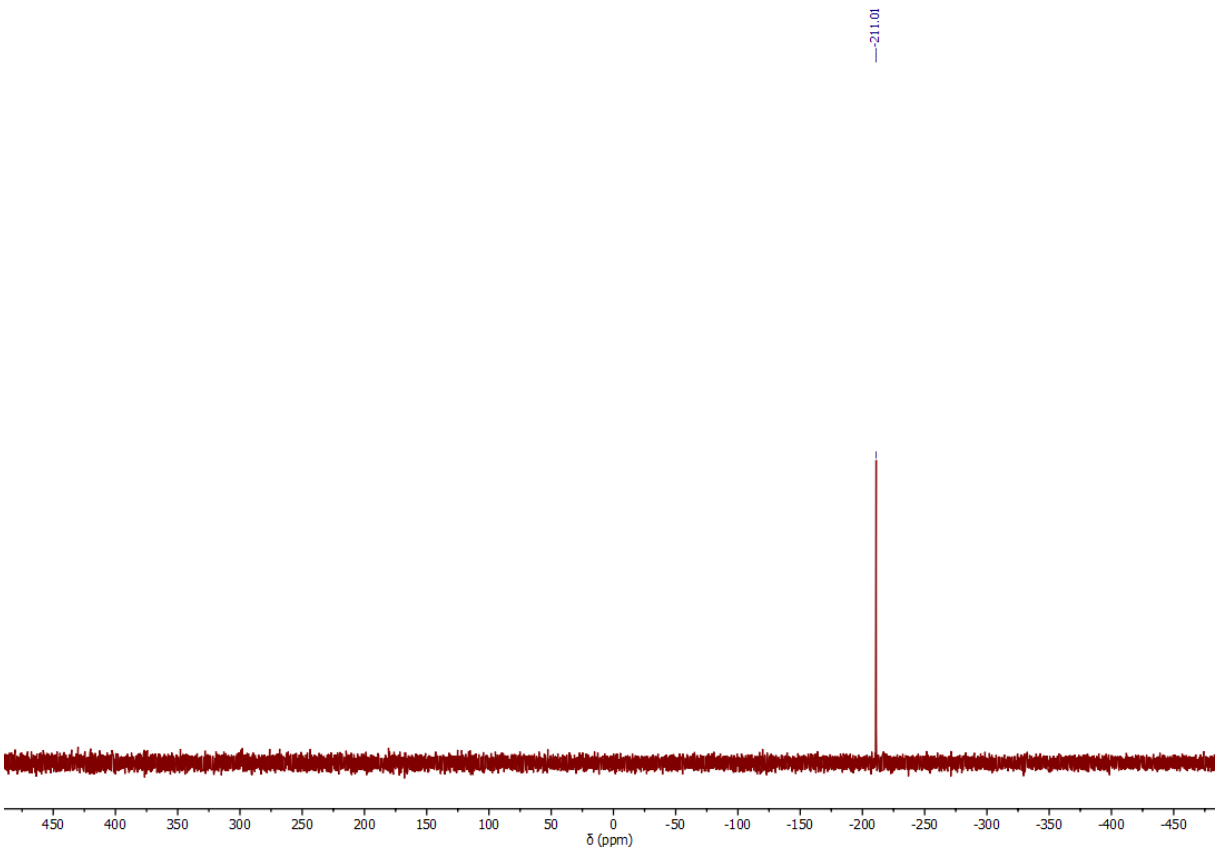

**Figure S35.** $^{119}Sn\{^{1}H\}$ NMR (224 MHz) spectrum of 5 in THF.

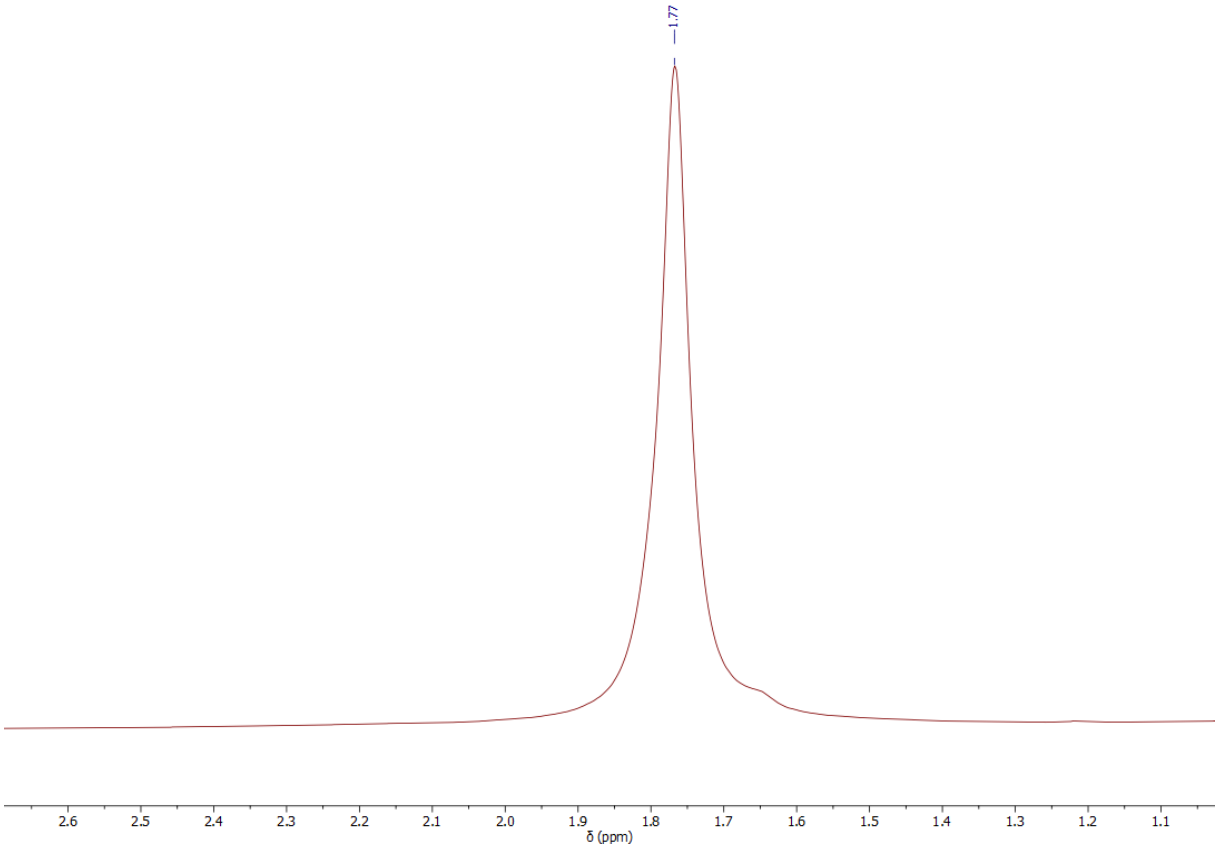


**Figure S36.** $^{7}Li$ NMR (233 MHz) spectrum of MeLi in THF.

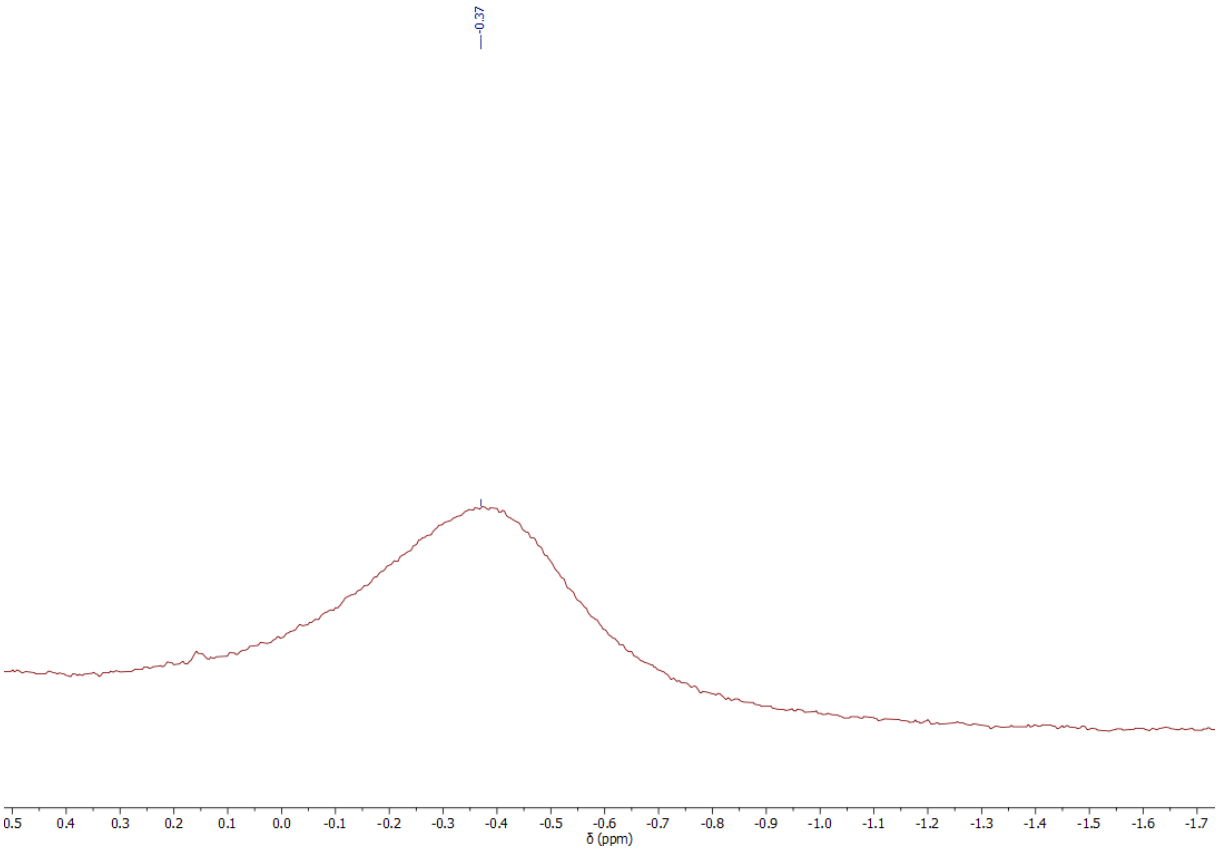


**Figure S37.** $^{7}$Li NMR (233 MHz) spectrum of 5 in THF.

# 6. Literature


[1] G. Sheldrick, *Acta Crystallographica Section A* **2008**, *64*, 112-122.

[2] L. Farrugia, *J. Appl. Crystallogr.* **1999**, *32*, 837-838.

[3] O. V. Dolomanov, L. J. Bourhis, R. J. Gildea, J. A. K. Howard, H. Puschmann, *J. Appl. Crystallogr.* **2009**, *42*, 339-341.

[4] J. Grolleau, P. Frère, F. Gohier, *Synthesis* **2015**, *47*, 3901-3906.

[5] U. Rosenthal, A. Ohff, W. Baumann, A. Tillack, H. Görls, V. V. Burlakov, V. B. Shur, *Z. anorg. allg. Chem.* **1995**, *621*, 77-83.

[6] S. Urrego-Riveros, I.-M. Ramirez y Medina, D. Duvinage, E. Lork, F. D. Sönnichsen, A. Staubitz, *Chem. Eur. J.* **2019**, *25*, 13318–13328.

[7] M. Saito, S. Imaizumi, T. Tajima, K. Ishimura, S. Nagase, *J. Am. Chem. Soc.* **2007**, *129*, 10974-10975.

[8] M. Saito, S. Imaizumi, T. Tajima, *Eur. J. Inorg. Chem.* **2010**, *2010*, 2153-2157.

[9] M. J. Frisch, G. W. Trucks, H. B. Schlegel, G. E. Scuseria, M. A. Robb, J. R. Cheeseman, G. Scalmani, V. Barone, B. Mennucci, G. A. Petersson, H. Nakatsuji, M. Caricato, H. P. H. X. Li, A. F. Izmaylov, J. Bloino, G. Zheng, J. L. Sonnenberg, M. Hada, M. Ehara, K. Toyota, R. Fukuda, J. Hasegawa, M. Ishida, T. Nakajima, Y. Honda, O. Kitao, H. Nakai, T. Vreven, J. A. Montgomery Jr., J. E. Peralta, F. Ogliaro, M. Bearpark, J. J. Heyd, E. Brothers, K. N. Kudin, V. N. Staroverov, R. Kobayashi, J. Normand, K. Raghavachari, A. Rendell, J. C. Burant, S. S. Iyengar, J. Tomasi, M. Cossi, N. Rega, J. M. Millam, M. Klene, J. E. Knox, J. B. Cross, V. Bakken, C. Adamo, J. Jaramillo, R. Gomperts, R. E. Stratmann, O. Yazyev, A. J. Austin, R. Cammi, C. Pomelli, J. W. Ochterski, R. L. Martin, K. Morokuma, V. G. Zakrzewski, G. A. Voth, P. Salvador, J. J. Dannenberg, S. Dapprich, A. D. Daniels, O. Farkas, J. B. Foresman, J. V Ortiz, J. Cioslowski, D. J. Fox, *Gaussian 16 Revision A.03, Gaussian, Inc., Wallingford CT* **2016**.

[10] A. D. McLean, G. S. Chandler, *J. Chem. Phys.* **1980**, *72*, 5639–5648.

[11] R. Krishnan, J. S. Binkley, R. Seeger, J. A. Pople, *J. Chem. Phys.* **1980**, *72*, 650–654.

[12] R. C. Binning Jr., L. A. Curtiss, *J. Comput. Chem.* **1990**, *11*, 1206–1216.

[13] M. P. McGrath, L. Radom, *J. Chem. Phys.* **1991**, *94*, 511–516.

[14] L. A. Curtiss, M. P. McGrath, J. Blaudeau, N. E. Davis, R. C. Binning, L. Radom, *J. Chem. Phys.* **1995**, *103*, 6104–6113.

[15] C. Adamo, V. Barone, *J. Chem. Phys.* **1999**, *110*, 6158–6170.

[16] S. Grimme, J. Antony, S. Ehrlich, H. Krieg, *J. Chem. Phys.* **2010**, *132*, 154104.

[17] S. Grimme, S. Ehrlich, L. Goerigk, *J. Comput. Chem.* **2011**, *32*, 1456–1465.

[18] G. Igel-Mann, H. Stoll, H. Preuss, *Mol. Phys.* **1988**, *65*, 1321–1328.

[19] A. Bergner, M. Dolg, W. Küchle, H. Stoll, H. Preuß, *Mol. Phys.* **1993**, *80*, 1431–1441.